DTIC FILE COPY

(1)

AD-A202 935

DTIC
ELECTE
JAN 18 1989
S D
H

DEPARTMENT OF THE AIR FORCE

AIR UNIVERSITY

AIR FORCE INSTITUTE OF TECHNOLOGY

Wright-Patterson Air Force Base, Ohio

DISTRIBUTION STATEMENT A
Approved for public release;
Distribution Unlimited

89 1 17 152

AFIT/MA/GE/88D-2

THE RADAR CROSS SECTION OF A TWO DIMENSIONAL DIELECTRIC COATED CYLINDER USING ON-SURFACE RADIATION CONDITIONS

THESIS

William D. Oetting
Captain, USAF

AFIT/MA/GE/88D-2

DTIC
ELECTE
JAN 18 1989
S H D

Approved for public release; distribution unlimited

AFIT/MA/GE/88D-2

THE RADAR CROSS SECTION OF A TWO DIMENSIONAL DIELECTRIC COATED CYLINDER USING ON-SURFACE RADIATION CONDITIONS

THESIS

Presented to the Faculty of the School of Engineering
of the Air Force Institute of Technology
Air University
In Partial Fulfillment of the
Requirements for the Degree of
Master of Science in Electrical Engineering

William D. Oetting, B.S.E.E.
Captain, USAF

December 1988

Approved for public release; distribution unlimited

Preface

The purpose of this study was to determine if the OSRC approximation technique could be applied to a coated scatterer and achieve reasonable accuracy. My original intentions were to do much more work with non-circular geometries than with circular geometries. However, as is the case so often in research projects, unexpected results and time limitations forced me to limit the class of problems considered to just circular geometries. The results presented here should be indicative of what may happen for a non-circular scatterer.

I am deeply indebted to my faculty advisor, Lt Col William Baker, for his assitance, patience and enthusiam. Col Baker's abiltity to transform mathematical symbols into an understanding of the behavior of the quantities represented by those symbols is truly unique. His enthusiam for his work was inspiring and helped me get through the difficult times when I was sick and tired of the project.

Finally, I want to thank my wife, [redacted], and son, [redacted] for their patience and understanding while I was tied to the computer for days and nights on end.

DTIC COPY INSPECTED

Accession For	
NTIS GRA&I	☑
DTIC TAB	☐
Unannounced	☐
Justification	
By	
Distribution/	
Availability Codes	
Dist	Avail and/or Special
A-1	

Table of Contents

List of Figures

Abstract

The purpose of this study was to use On-Surface Radiation Conditions (OSRC) to approximate the RCS of a two dimensional dielectric coated circular cylinder and compare the results to an exact solution. The comparisons were made to determine a lower and/or upper bound on the frequency, radius of curvature of the cylinder or any other pertinent parameters for a valid approximation.

The problem was formulated for a circular cylinder of radius a coated by a lossy dielectric of radius b and a unit magnitude plane wave incident from the ϕ = 180 degrees direction with wave number k. The OSRC solution and the eigenfunction solution were nearly identical; however, the overall accuracy of the OSRC technique was shown to be governed by a complicated expression which was dependent on the dielectric material parameters as well as the kb product. The solutions were compared for three different circumstances: fixed frequency and varying dielectric layer thickness; fixed geometry and varying frequency; fixed frequency and geometry and bistatic RCS. The OSRC solution was said to be good if the error was less than 2 db.

The OSRC solution was found to agree with the eigenfunction solution for wide ranges of parameters. In

general these parameters were the thickness of the dielectric layer less than 0.4 wavelengths for TM polarization, the magnitude of the imaginary part of the relative permittivity greater than 1.0 for incident TM polarization or 1.5 for incident TE polarization, or the kb product "very" large. Data was presented which precisely outlined which combinations of geometry, dielectric material loss, polarization and frequency produced a valid OSRC approximation.

These results are consistent with the physical behavior of the field in the dielectric layer. The OSRC technique was shown to be inaccurate for higher order modes. Whenever a situation was examined which would be likely to excite higher order modes, the error in the OSRC solution was large. For instance, TE polarization is much more likely to excite traveling waves along the surface of the conducting cylinder. These traveling waves are higher order modes of the field in the dielectric layer. Data was presented which showed that the error in the OSRC solution was greater for TE polarization than for TM polarization, for identical geometries and frequencies, due to the contribution of these higher order modes.

THE RADAR CROSS SECTION OF A TWO DIMENSIONAL DIELECTRIC COATED CYLINDER USING ON-SURFACE RADIATION CONDITIONS

I. Introduction

Background

Exact analytical solutions for electromagnetic scattering and diffraction phenomena are limited to a small class of simple shapes whose surfaces coincide with those of an orthogonal curvilinear coordinate system. Use of a digital computer makes it possible to obtain rigorous numerical solutions for electrically small structures of arbitrary shape using an integral equation formulation. However, due to the finite capacity of the computer this method becomes untenable as the frequency increases (James, 1974:1). These constraints on solving scattering problems have given rise to many different approximation techniques. Ruck and others describe several different approximation techniques for computing the scattered fields and thus the radar cross section (RCS) of structures which are not amenable to exact solutions. Most notable are physical optics (PO), geometrical optics (GO) and the geometrical theory of diffraction (GTD) (Ruck and others, 1970:39-105 and Jost,

1988). Other techniques which have been used to improve on these high frequency approximations are physical theory of diffraction (PTD) and uniform theory of diffraction (UTD) (James, 1974:4 and Leader, 1982:19). Many new techniques and variations of these techniques appear in the literature every year.

A new high frequency technique, which has been named On-Surface Radiation Conditions (OSRC), has been shown to produce an analytical approximation for the RCS of several two dimensional perfectly conducting bodies (Kriegsmann and others, 1987:153-155). The purpose of this study was to use OSRCs to approximate the RCS of a two dimensional dielectric coated circular cylinder and compare the results to an exact solution to determine the validity of the method.

Problem Statement

The RCS of a two dimensional, perfectly conducting, circular cylinder coated with a lossy dielectric material will be found using On-Surface Radiation Conditions. This approximate solution will be compared to the exact solution, for circular geometries, to determine a lower and/or upper bound on the frequency, radius of curvature of the cylinder or any other pertinent parameter for a valid approximation. Any improvement in computational efficiency will also be measured.

Summary of OSRC Method

The OSRC technique uses the asymptotic behavior of the appropriate Green's function to establish a series of differential operators that annihilate the first N terms of the asymptotic series of the scattered field (Kriegsmann and others, 1987:153).

Kriegsmann and Morawetz first derived the differential operators to be used in this investigation (Kriegsmann and Morawetz, 1980:371-385); however, the operators were applied at some distance off the surface of the scatterer. The interested reader is referred to this paper for the details of the derivation. Kriegsmann and others were the first to apply these differential operators directly on the surface of the scattering body (Kriegsmann and others, 1987:153-155). Their problem was formulated using the free space Green's function to write a surface integral equation for the scattered field. As usual, both the scattered field and its first derivative with respect to the surface normal appeared in the integrand. However, since the scatterer was perfectly conducting, the scattered field was replaced by the negative of the incident field evaluated on the surface of the scattering body. The problem was thus reduced to finding an expression for the normal derivative of the scattered field on the surface of the scatterer. Application of a differential operator to the asymptotic

series for the scattered field produces an approximation for this derivative which is accurate to order $R^{(-2N-1/2)}$, where N is the order of the operator and R is the vector magnitude of the distance from the surface of the scatterer to the origin. The order of the operator implies that it annihilates the first N terms of the asymptotic series for the scattered field. The expression for the normal derivative was substituted into the integral equation and a far field expansion for the Green's function produced an asymptotic series for the scattered field. The surface electric current density was found to be proportional to the sum of the normal derivatives of the scattered and incident fields. The scattering cross section was found to be proportional to the magnitude squared of the first coefficient of the asymptotic series representing the scattered field (Kriegsmann and others, 1987:154-155).

Kriegsmann and others used the first (B_1) and second (B_2) order operators to solve for the scattering cross section and surface currents of several perfectly conducting geometries. The first three examples were for TM polarization and the last example was for TE polarization.

The bistatic RCS for a circular cylinder was compared to the exact solution and found to agree to within 0.5 dB for B_2 and to significantly disagree for B_1. The OSRC solution, using B_2, required the evaluation of only two Bessel

functions regardless of the electrical size of the cylinder. Additionally, both OSRC solutions produced a non-zero surface current in the shadow region of the cylinder. This was shown to be significantly closer to the exact solution than the physical optics solution for the surface currents. Next, the OSRC technique, using B_2 only, was applied to a conducting strip to find the monostatic cross section. This solution was compared to a method of moments (MM) solution and found to be within 1 dB for angles of incidence within thirty degrees of broadside, except at nulls. Disagreement at grazing angles was attributed to edge currents. Then the OSRC approximation was found to agree within 0.5 dB with a moment method solution for the cross section of a square conducting cylinder for angles of incidence within 45 degrees of broadside. Finally, the surface current density for a circular cylinder with incident TE polarization using B_1 and B_2 was compared to a moment method solution. Again the B_2 solution was found to agree very well with the MM solution and produce a non-zero current in the shadow region of the cylinder. In all the cases presented above, an analytical expression for the surface current or scattering cross section was derived and the expressions for the surface currents remained valid across the shadow boundary (Kriegsmann and others, 1987:155-159).

Approach

Two approximations for the RCS using OSRC will be presented. Both solutions use the two dimensional Green's function to write an integral equation for the scattered field. The first method uses the boundary conditions at the interface between the dielectric layer and free space to express the integration in terms of the incident field and the field in the dielectric material. Since the incident field is known, the OSRC technique will be used to approximate the field in the dielectric material. The second method uses the OSRC technique combined with the boundary conditions to express the integral in terms of the incident field and the field in the dielectric material. Both methods use the asymptotic behavior of the Green's function to derive a far field expression for the scattered field from the integral equation.

The bistatic RCS of a dielectric coated circular cylinder will be found using the approach described above. Both OSRC solutions will be compared to the exact series solution for this geometry (Tang, 1957:639-630). Agreement between the two solutions will be considered a validation of the OSRC solution for the ranges of parameters compared.

Assumptions

The discussion presented above is based on several

assumptions. First, all fields are time harmonic; an exp(-jwt) time dependence will be assumed throughout. Next, the inner cylinder is perfectly conducting and the dielectric material is homogeneous. Finally, the surface charge and current density of the coating material are assumed to be zero. These assumptions are standard for this class of problem.

Notation

A consistent set of notation was used throughout the study. An underlined quantity is generally a vector quantity. A primed (') coordinate is the integration coordinate and an unprimed coordinate is the observation coordinate. The cylindrical coordinate system was used for all the derivations presented. Specifically, some of the symbols used are:

$\underline{E}$ = Electric field vector

$\underline{H}$ = Magnetic field vector

$\underline{r}$ = posistion vector

$\cdot$ = dot product

X = cross product

∇ = Laplacian operator

r = distance from z axis

θ = angular rotation from x axis

Φ = z component of $\underline{E}$ or $\underline{H}$ field

ϵ_o = permittivity of free space

μ_o = permeability of free space

ϵ_r = relative permittivity

μ_r = relative permeability

n_o = index of refraction

σ = conductivity

k = wave number

w = radian frequency

Summary

An approximation for the RCS of a two dimensional, perfectly conducting cylinder coated with a lossy dielectric material will be derived using two equivalent OSRC methods. The results from this analysis will be compared to the series solution and the range of validity of the OSRC technique will be investigated. In addition, the OSRC solution for this problem will be shown to reduce to the OSRC solution for a perfectly conducting cylinder as the thickness of the dielectric layer goes to zero. The OSRC technique has shown excellent results when applied to several two dimensional perfectly conducting bodies. The OSRC approximation was, in general, accurate to within 1 dB using the second order boundary operator.

II. Review of Literature

Introduction

Applying a radiation condition at infinity has been used for decades to solve for the scattered fields from objects where the geometry allows the investigator to derive an analytical solution. For geometries where a numerical solution is required a finite region must be artificially introduced to make the problem feasible for computer application. Over the years, several techniques have been developed which accomplish this feat with reasonable degrees of accuracy and varying degrees of difficulty. The OSRC technique consists of the application of higher order differential operators to the far field expression for the scattered field to truncate the numerical solution. Kriegsmann and others noted that the use of higher order differential operators appears to fall into two categories. The first uses the asymptotic behavior of the appropriate Greens function to establish a series of operators that annihilate the first n terms of the asymptotic series of the scattered field (Kriegsmann and others, 1987:153). They describe the second category as follows:

> The second category . . . derives an approximate one-way wave equation in Cartesian coordinates by factoring

> the dispersion relation of the full wave equation, and providing a rational polynomial interpolation of the resulting square root at selected wave propagation angles. This results in reflection free passage of the plane waves propagating at these angles through the lattice truncation plane. The number of reflection free angles and their values can be selected in a systematic manner [Kriegsmann and others, 1987:153].

The OSRC technique to be used here falls into the first category. Before beginning the derivation of the OSRC solution, a few of the other techniques used to solve this problem will be reviewed.

Summary of Other Techniques

This problem has been solved using a vast number of different techniques. A few of the more pertinent techniques will be discussed. The first technique to be presented is the eigenfunction expansion solution followed by a recently published geometrical optics solution. Then several of the more recently published numerical approximations will be presented. These techniques include the method of moments (MM), the unimoment method and a hybrid finite element method.

Eigenfunction Expansion. For a circular cylinder covered with a circular dielectric layer, the normal boundary conditions and the radiation condition at infinity, Tang used the eigenfunction expansion method to solve the system

of partial differential equations for the backscattered field. The solution consists of an infinite series of Hankel functions, in which the constants are ratios of sums of Bessel functions and their derivatives, evaluated on the conducting and dielectric surfaces. Tang found excellent agreement between this solution and measured values for the cases presented below (Tang, 1957:628-630).

$ka = 0.942, \quad 1.5 \leq k_2 b \leq 10, \quad \epsilon_r = 2.54$

$ka = 2.0, \quad 3.188 < k_2 b \leq 10, \quad \epsilon_r = 2.54$

$ka = 3.5, \quad 5.58 \leq k_2 b \leq 10, \quad \epsilon_r = 2.54$

$ka = 0.942, \quad 2.308 \leq k_2 b \leq 10, \quad \epsilon_r = 6$

$ka = 1.302, \quad 3.188 \leq k_2 b \leq 10, \quad \epsilon_r = 6$

where,

k = wave number in free space

k_2 = wave number in the dielectric

a = radius of the conductor

b = radius of the dielectric

ϵ_r = relative permittivity (Tang, 1957:628-630)

Since this solution is a strict mathematical solution to the partial differential equations it can be called the exact solution for the circular geometry case.

Geometrical Optics. Wang has used a Watsons transformation on the eigenfunction solution to approximate the scattered field from a dielectric coated circular

cylinder as the sum of a geometrical optics or ray solution and two surface waves. Numerical results were compared to the eigenfunction solution and found to be in excellent agreement for ka greater than 2.0 and the thickness of the dielectric coating less than 0.41 wavelengths (Wang, 1985:960-963).

Method of Moments. The method of moments (MM) has been used to solve the dielectric cylinder problem by Wu and Tsai. They formulated the problem for arbitrary shaped conductor and dielectric coating as a system of coupled surface integral equations derived from Maxwell's equations, Green's theorem and the appropriate boundary conditions for transverse electric (TE) or transverse magnetic (TM) polarization. The radiation conditions were incorporated into the formulation via the free space Green's function. They solved the system of the integral equations using flat pulse expansion functions and point matching. Several examples of dielectric cylinders and dielectric coated conducting cylinders were given. The circular geometry dielectric coated conducting cylinder solution was compared to Tang's solution. (Wu and Tsai, 1977:519-522).

For the lossless dielectric case, Wu and Tsai found excellent agreement between the MM solution and Tang's eigenfunction solution for the backscattered cross section for the case ka = 0.942, ϵ_r = 2.54 and $2 \leq kb \leq 7$. In

addition to the lossless case, they computed the cross section for the conductivity (σ) of the dielectric equal to 0.01 and 0.05 mho/meter. It was concluded that the effect of a lossy dielectric was to significantly dampen RCS oscillations (Wu and Tsai, 1977:522).

Another example that is relevant here is the circular cylinder enclosed in a dielectric wedge semi-circle. Figure 1 shows the geometry and MM solution for this problem. The dotted lines indicate regions where the solution was extrapolated due to numerical instabilities in the matrix inversion. Wu and Tsai found that the numerical instabilities occurred whenever an interior resonance occurred and that the condition number was an excellent indicator of this instability (Wu and Tsai, 1977:520-523). This seems to be an inherent limitation of the MM technique.

Unimoment Method. Chang and Mei have applied unimoment methods to the dielectric cylinder problem. The unimoment method involves enclosing the cylinder in an artificial boundary, usually a circle for two dimensional problems, and enforcing boundary conditions of the $\underline{E}$ and $\underline{H}$ fields on this artificial boundary instead of the actual dielectric boundary. The total field inside of this boundary is expressed as a finite sum of unknown constants multiplying a set of expansion functions and the scattered field outside of this boundary is approximated by a finite series of

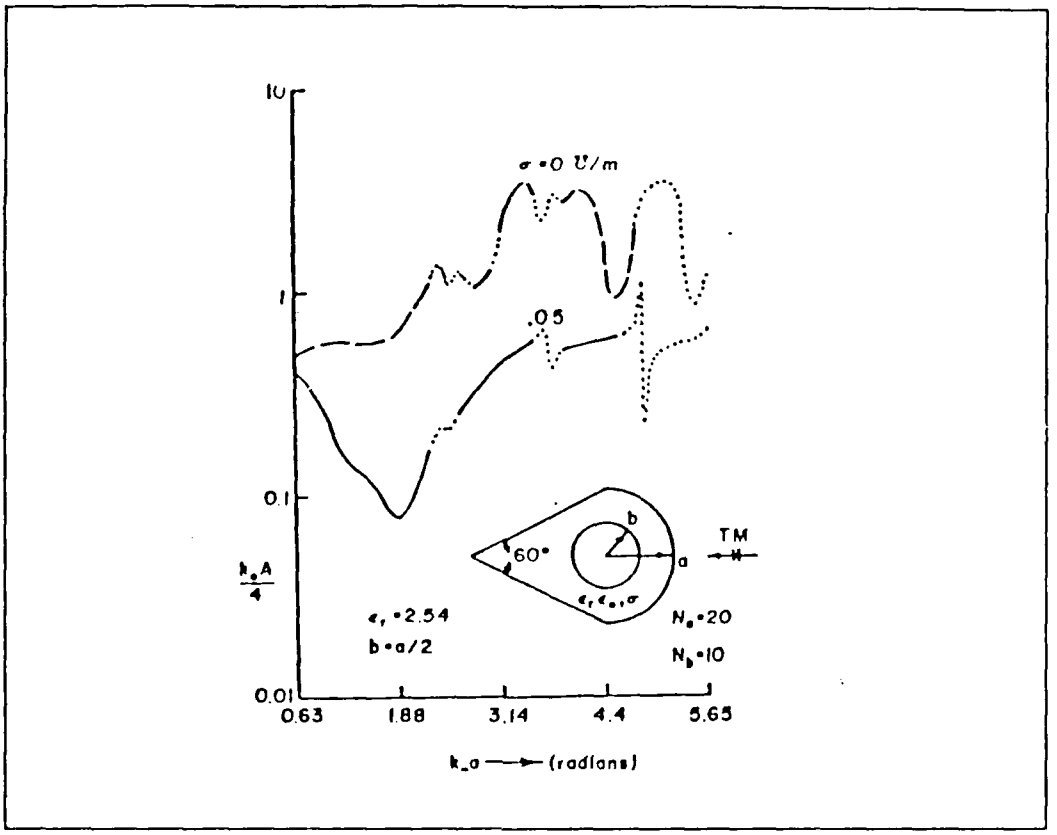

Figure 1. Backscattered RCS of a Conducting Circular Cylinder Enclosed in a Dielectric Wedge-Semicircle (Wu and Tsai, 1977:522)

Hankel functions. The incident field is generally assumed to be a plane wave. For two dimensional problems the obvious choice of expansion functions, for the field inside of the boundary, that satisfy periodicity conditions are sinusoids. Finite element methods are used inside of the artificial boundary to solve for the total field on the surface of the boundary. The continuity of the E or H fields across this boundary is used to relate the constants

of the two series expansions, thus solving for the scattered field or scattering cross section. Chang and Mei used this technique to solve for the scattered field from an off center, circular, dielectric cylinder and other geometries and found excellent agreement between their solution and the normal series solution obtained from separation of variables (Chang and Mei, 1976:35-39).

Hybrid Finite Element Methods. As illustrated by Chang and Mei above, finite element methods can be used to solve field problems in unbounded regions. However, imposing artificial boundaries is not efficient when dealing with noncircular geometries (Jin and Liepa, 1988:50). As implemented by Jin and Liepa, the hybrid finite element method (HFEM) encloses the scatterer in two artificial boundaries that match the surface of the scatterer. This reduces the region in which a numerical solution must be found. Figure 2 shows the general problem formulation used by Jin and Liepa. They describe the technique as follows:

> The basic idea of the method is to draw one artificial boundary Γ_A enclosing Γ_D and another artificial boundary Γ_B lying between Γ_A and Γ_D. To minimize the region treated by FEM, Γ_A is drawn in such a way that only one layer of triangular elements is needed between Γ_A and Γ_D. We will use FEM in the region R_I defined by Γ_A and Γ_C, and use free-space Green's function integral formulation in the region outside Γ_A [Jin and Liepa, 1988:51].

Jin and Liepa found good agreement between their solution for the far field factor (Bowman and others, 1969:6) for a

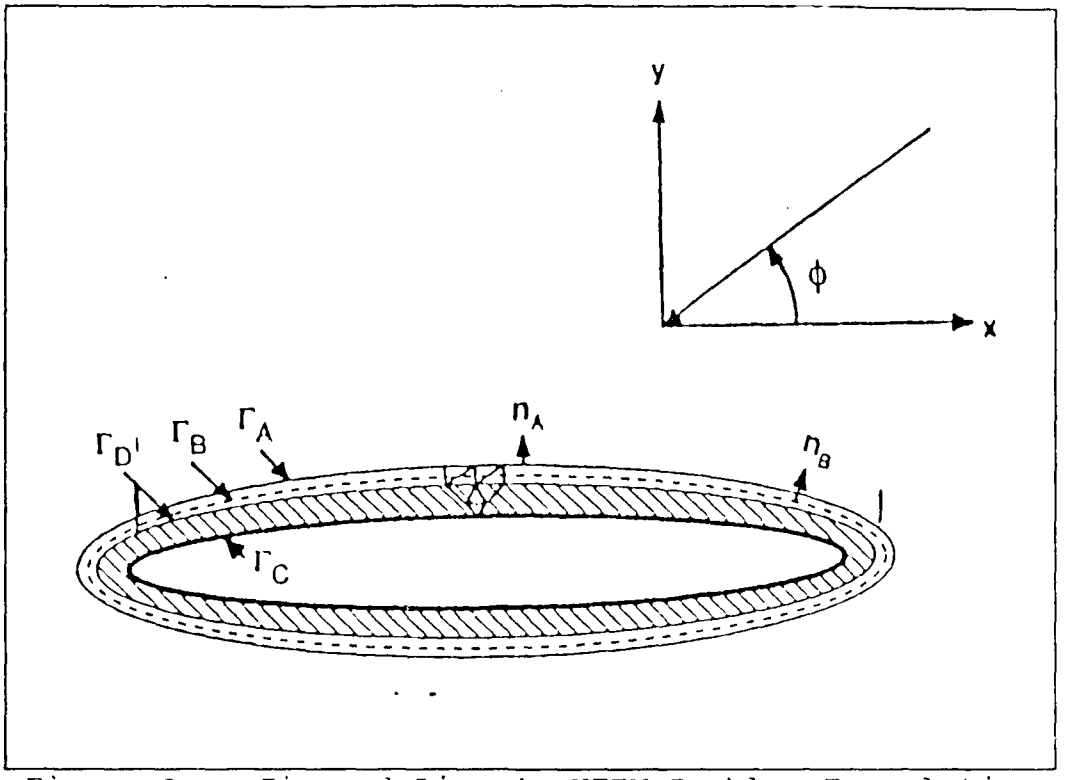

Figure 2. Jin and Liepa's HFEM Problem Formulation (Jin and Liepa, 1988:51)

circular cylinder coated with a circular dielectric/magnetic material and the eigenfunction expansion (Tang, 1957:628-630) or the method of moments with impedance boundary conditions. In addition, they compared the efficiency and accuracy of the HFEM solution to a volume moment method solution for the same geometry but with a dielectric material only (Jin and Liepa, 1988:52). They summarize the results as follows:

> Comparison shows that HFEM has essentially the same accuracy as MM in this E-polarized case. However,

> using MM in the case of H-polarization, one would have to compute both the normal and tangential equivalent electric current components and thus have a larger resultant matrix . . . [Jin and Liepa, 1988:52].

They also concluded that with HFEM the size of the matrix remains the same if the coating material is magnetic as well as dielectric while with MM the matrix size will increase by approximately a factor of three (Jin and Liepa, 1988:52).

Summary

Several different methods for solving for the scattering cross section of a dielectric coated conducting cylinder were reviewed. In general, if the geometry did not match a set of orthogonal coordinates, a numerical technique must be applied to the problem. Introducing an artificial boundary is one numerical method that has been successfully used (Chang and Mei, 1976:35-42) and work has been done on improving the efficiency of this technique (Jin and Liepa, 1988:50-54). However, the OSRC method takes advantage of the natural boundaries of the system to derive an approximation for the cross section or surface currents. Its advantage is simplicity and a consistent ease of application for arbitrary convex cylinders (Kriegsmann and others, 1987:160). Application of the OSRC method to a dielectric coated cylinder is not evident in the literature and should prove to be a natural extension to the previously published work with this technique.

III. Problem Formulation and Solution

Introduction

The radar cross section (RCS) of a two dimensional object can be thought of as the cross section per unit length and has been called the scattering width (Knott and others, 1985:157) or the echo area (Peters, 1958:133). For our purposes, RCS will mean the two dimensional RCS and is defined as (Bowman and others, 1969:7):

$$\sigma = \lim_{r\to\infty} 2\pi r \frac{|\underline{E}^s|^2}{|\underline{E}^i|^2} = \lim_{r\to\infty} 2\pi r \frac{|\underline{H}^s|^2}{|\underline{H}^i|^2} \quad (3.1)$$

where,

r = radial distance from the z axis

$\underline{E}^s$ = scattered electric field

$\underline{H}^s$ = scattered magnetic field

$\underline{E}^i$ = incident electric field

$\underline{H}^i$ = incident magnetic field

Since the incident field is assumed to be a unit magnitude plane wave, the problem of determining the RCS reduces to finding an expression for the scattered fields.

Starting with Maxwell's equations, the equations for the fields scattered from a dielectric coated, infinite cylinder will be formulated for arbitrary geometries using transverse

magnetic (TM) and transverse electric (TE) polarizations. TM polarization implies the incident electric field is polarized parallel to the cylinder axis only while TE polarization implies the incident magnetic field is polarized parallel to the cylinder axis. These equations can be solved exactly for a right circular cylinder coated with a circular layer of dielectric material and this solution will be presented. The OSRC approximation to the scattered fields will be derived for this special geometry and this approximate solution will be compared to the exact solution. The cylindrical coordinate system will be used throughout this analysis..

Problem Formulation

Figure 3 shows the arbitrary geometry problem, a perfectly conducting cylinder coated by a layer of dielectric material with relative permittivity ϵ_r, relative permeability μ_r and conductivity σ. $\underline{E}$ and $\underline{H}$ are the total electric and magnetic fields in Region I, free space. $\underline{E}^D$ and $\underline{H}^D$ are the electric and magnetic fields in Region II, the dielectric material. The fields in Region I consist of an incident plane wave traveling in the $\hat{x}$ direction ($\underline{E}^i$, $\underline{H}^i$) and the fields scattered from the dielectric coated cylinder ($\underline{E}^s$, $\underline{H}^s$). Γ_1 is the surface of the dielectric/conductor boundary and Γ_2 is the surface of the dielectric/free space

boundary.

Assuming an exp(-jwt) time dependence, Maxwell's equations can be written as:

$$\text{curl}\underline{E} = jw\mu_r\mu_o\underline{H} \quad \text{and} \quad \text{curl}\underline{H} = -(\sigma + jw\epsilon_r\epsilon_o)\underline{E}$$

Taking the curl of both equations, substituting the original equations into the new equations and rearranging terms yields the homogenous vector wave equation for the electric or magnetic field in an linear, homogenous, isotropic medium (Harrington, 1961:37).

$$\text{curlcurl}\underline{E} - (kn_o)^2\,\underline{E} = 0 \qquad (3.2a)$$

$$\text{curlcurl}\underline{H} - (kn_o)^2\,\underline{H} = 0 \qquad (3.2b)$$

where,

$$k = \text{wave number} = w(\epsilon_o\mu_o)^{1/2}$$

$$n_o = \text{complex index of refraction} = \{\epsilon_r\mu_r(\,1 + j\sigma/(w\epsilon_r\epsilon_o)\,)\}^{1/2}$$

$$w = \text{radian frequency}$$

For TM polarization, the electric field is expressed as $\underline{E} = (\,0,\ 0,\ \Phi\,)$ and the electric field equations are used to solve for the RCS. For TE polarization the magnetic field is expressed as $\underline{H} = (\,0,\ 0,\ \Phi\,)$ and the magnetic field equations are used to solve for the RCS. Substituting these field representations into the vector wave equations above yields the scalar Helmholtz equation for both polarizations.

$$f\Phi + (kn_o)^2\,\Phi = 0 \qquad (3.3)$$

where f is the Laplacian operator and Φ is the z component of the electric field for TM polarization or Φ is the z

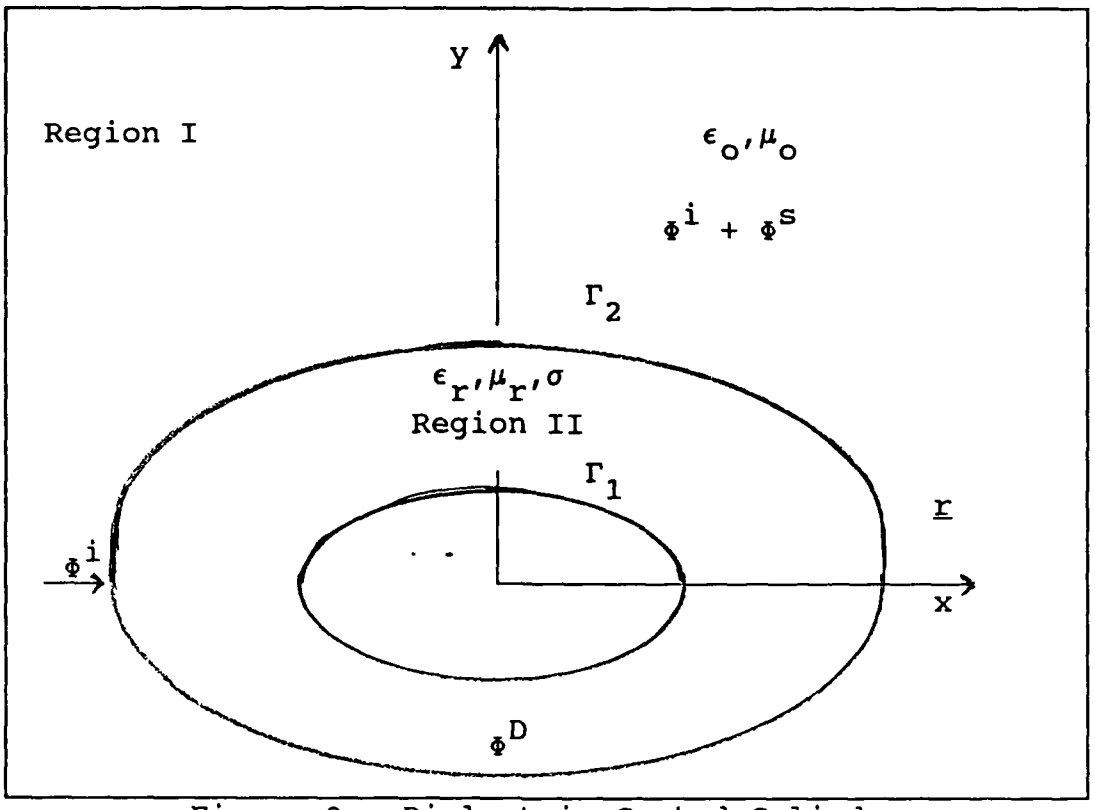

Figure 3. Dielectric Coated Cylinder

component of the magnetic field for TE polarization. It is implicit in Equation 3.3 that div$\underline{E}$ = div$\underline{H}$ = 0 (e.g. the medium has zero charge density).

In Region II $\Phi = \Phi^D$, where Φ^D is the total field in the dielectric material and Φ^D satisfies Equation 3.3. In Region I, $\Phi = \Phi^i + \Phi^s$ and $n_o = 1$, where Φ^i and Φ^s are the scalar components of the incident and scattered fields respectively. Substituting into Equation 3.3 yields:

$$f\Phi^i + k^2\Phi^i + f\Phi^s + k^2\Phi^s = 0 \qquad (3.4)$$

However, since Φ^i exists whether or not the scattering

object is present, it must satisfy Equation 3.3 by itself. Therefore, Equation 3.4 reduces to:

$$\nabla\Phi^s + k^2\Phi^s = 0 \qquad (3.5)$$

In addition to Equations 3.3 and 3.5, the boundary conditions at Γ_1 and Γ_2 are needed to find a unique solution for the scattered fields.

The boundary conditions at Γ_1 are:

$$\hat{n} \times \underline{E} = 0 \qquad (3.6a)$$

$$\hat{n} \times \underline{H} = \underline{J}^s \qquad (3.6b)$$

$$\hat{n} \cdot \underline{E} = p_s/\epsilon_r \qquad (3.6c)$$

$$\hat{n} \cdot \underline{H} = 0 \qquad (3.6d)$$

The boundary conditions at Γ_2 are:

$$\hat{n} \times \underline{E} = \hat{n} \times (\underline{E}^i + \underline{E}^s) = \hat{n} \times \underline{E}^D \qquad (3.7a)$$

$$\hat{n} \times \underline{H} = \hat{n} \times (\underline{H}^i + \underline{H}^s) = \hat{n} \times \underline{H}^D \qquad (3.7b)$$

$$\hat{n} \cdot \underline{E} = \hat{n} \cdot (\underline{E}^i + \underline{E}^s) = \epsilon_r (\hat{n} \cdot \underline{E}^D) \qquad (3.7c)$$

$$\hat{n} \cdot \underline{H} = \hat{n} \cdot (\underline{H}^i + \underline{H}^s) = \mu_r(\hat{n} \cdot \underline{H}^D) \qquad (3.7d)$$

where,

$\hat{n}$ = unit vector normal to the respective surface

$\underline{J}^s$ = surface current vector

p_s = surface electric charge density

For incident TM polarization, Equations 3.6a, 3.7a and 3.7b reduce to:

$$\Phi^D = 0 \qquad \text{on } \Gamma_1 \qquad (3.8a)$$

$$\Phi^i + \Phi^s = \Phi^D \qquad \text{on } \Gamma_2 \qquad (3.8b)$$

$$\frac{\delta \Phi^i}{\delta \hat{n}} + \frac{\delta \Phi^s}{\delta \hat{n}} = \frac{1}{\mu_r} \frac{\delta \Phi^D}{\delta \hat{n}} \quad \text{on } \Gamma_2 \qquad (3.8c)$$

For incident TE polarization, equations 3.6b, 3.7a and 3.7b reduce to:

$$\frac{\delta \Phi^D}{\delta \hat{n}} = 0 \quad \text{on } \Gamma_1 \qquad (3.9a)$$

$$\Phi^i + \Phi^s = \Phi^D \quad \text{on } \Gamma_2 \qquad (3.9b)$$

$$\frac{\delta \Phi^i}{\delta \hat{n}} + \frac{\delta \Phi^s}{\delta \hat{n}} = \frac{1}{\epsilon_r} \frac{\delta \Phi^D}{\delta \hat{n}} \quad \text{on } \Gamma_2 \qquad (3.9c)$$

Equations 3.3, with $\Phi = \Phi^D$, 3.5 and 3.8 form the complete problem for incident TM polarization, while Equations 3.3, 3.5 and 3.9 form the complete problem for incident TE polarization.

In order to implement the OSRC technique it is necessary to express Equation 3.5 in its integral equation form using Green's Theorem and the two dimensional free space Green's function for the scalar Helmholtz equation. Using these techniques, Equation 3.5 can be recast as:

$$\Phi^s = \int_{\Gamma_2} \left[G(\underline{r},\underline{r}') \frac{\delta \Phi^s}{\delta \hat{n}} - \Phi^s \frac{\delta G(\underline{r},\underline{r}')}{\delta \hat{n}} \right] \delta s' \qquad (3.10)$$

where,

$$G(\underline{r},\underline{r}') = \text{Green's function} = \frac{j}{4} H_0^{(1)}(k|\underline{r} - \underline{r}'|)$$

and $H_n^{(1)}(x)$ is a Bessel function of the third kind or Hankel function. The boundary conditions (Equations 3.8b

and 3.8c for incident TM polarization or Equations 3.9b and 3.9c for incident TE polarization) can be used to substitute for the scattered field and its normal derivative in the integrand of Equation 3.10. Thus, the expression for the scattered field becomes:

$$\Phi^s = \int_{\Gamma_2} \left[G(\underline{r},\underline{r}') \frac{1}{p_r} \frac{\delta \Phi^D}{\delta \hat{n}} - \Phi^D \frac{\delta G(\underline{r},\underline{r}')}{\delta \hat{n}} \right] \delta s'$$

$$- \int_{\Gamma_2} \left[G(\underline{r},\underline{r}') \frac{\delta \Phi^i}{\delta \hat{n}} - \Phi^i \frac{\delta G(\underline{r},\underline{r}')}{\delta \hat{n}} \right] \delta s' \quad (3.11)$$

where p_r is μ_r for TM polarization or ϵ_r for TE polarization.

Exact Solution for Circular Geometries

For Γ_2 a circle of radius b and Γ_1 a circle of radius a, where $b \geq a$, the normal derivatives in all of the above equations become derivatives with respect to r', the radial coordinate. Thus, Equation 3.11 becomes:

$$\Phi^s = b \int_0^{2\pi} \left[G(\underline{r},\underline{r}') \frac{1}{p_r} \frac{\delta \Phi^D}{\delta r'} - \Phi^D \frac{\delta G(\underline{r},\underline{r}')}{\delta r'} \right] \delta \theta'$$

$$- b \int_0^{2\pi} \left[G(\underline{r},\underline{r}') \frac{\delta \Phi^i}{\delta r'} - \Phi^i \frac{\delta G(\underline{r},\underline{r}')}{\delta r'} \right] \delta \theta' \quad (3.12)$$

Since we are interested in the behavior of the scattered field as r goes to infinity, the first term of the

asymptotic expansion of the Green's function and its derivative can be used in Equation 3.12. These expansions are:

$$G(\underline{r},\underline{r}') \sim G_0 \, e^{-jkr'\cos(\theta - \theta')} \tag{3.12a}$$

$$\frac{\delta G(\underline{r},\underline{r}')}{\delta r} \sim -jkG_0\cos(\theta - \theta') \, e^{-jkr'\cos(\theta - \theta')} \tag{3.12b}$$

where,

$$G_0 = \frac{e^{j(kr + \pi/4)}}{(8\pi kr)^{1/2}} \tag{3.12c}$$

Substituting Equations 3.12a and 3.12b into Equation 3.11 yields:

$$\Phi_f^s = bG_0 \int_0^{2\pi} \left[\frac{1}{p_r} \frac{\delta \Phi^D}{\delta r'} + jk\cos(\theta - \theta') \, \Phi^D \right] e^{-jkb\cos(\theta - \theta')} d\theta'$$

$$- bG_0 \int_0^{2\pi} \left[\frac{\delta \Phi^i}{\delta r'} + jk\cos(\theta - \theta') \, \Phi^i \right] e^{-jkb\cos(\theta - \theta')} \, d\theta' \tag{3.13}$$

where Φ_f^s is the far field approximation for Φ^s.

The incident field is assumed to be a unit magnitude plane wave traveling in the positive x direction. This can be expressed as the normal complex exponential function or as a series of cylindrical wave functions (Harrington, 1961:231):

$$\Phi^i = e^{jkx} = e^{jkr\cos(\theta)} = \sum_{n=-\infty}^{n=\infty} j^n \, J_n(kr) \, e^{jn\theta} \tag{3.14}$$

Now it is necessary to solve Equation 3.3 to find an

expression for Φ^D to use in the integrand of Equation 3.13.

The method of eigenfunction expansion will be used to solve for Φ^D and Φ^S for either polarization. Any linear combination of Bessel functions will suffice as an eigenfunction for Equation 3.3 (Baker, 1988). However, Hankel functions were chosen because they exhibit the correct behavior for traveling wave solutions. Thus, the eigenfunctions are:

$H_n^{(1)}(x)$ = outward going wave solution = $J_n(x) + j\ Y_n(x)$

$H_n^{(2)}(x)$ = inward going wave solution = $J_n(x) - j\ Y_n(x)$

where $J_n(x)$ are Bessel functions of the first kind and $Y_n(x)$ are Bessel functions of the second kind.

In additional to the boundary conditions, all the field solutions must satisfy periodicity conditions with respect to and the scattered field must satisfy the Sommerfeld radiation conditions.

Thus the solution for Φ^D may be written as:

$$\Phi^D = \sum_{n=-\infty}^{n=\infty} j^n \left(A_n H_n^{(1)}(kn_o r) + B_n H_n^{(2)}(kn_o r) \right) e^{jn\theta} \quad (3.15)$$

and the solution for Φ^S may be written as:

$$\Phi^S = \sum_{n=-\infty}^{n=\infty} j^n C_n H_n^{(1)}(kr)\ e^{jn\theta} \quad (3.16)$$

where A_n, B_n, and C_n are the unknown coefficients.

Enforcing the boundary conditions at Γ_1 and Γ_2 yields:

$$B_n = - A_n \frac{H_n^{(1)}(kn_o a)}{H_n^{(2)}(kn_o a)} \quad \text{for TM polarization} \qquad (3.17a)$$

$$B_n = - A_n \frac{\dot{H}_n^{(1)}(kn_o a)}{\dot{H}_n^{(2)}(kn_o a)} \quad \text{for TE polarization} \qquad (3.17b)$$

$$A_n = \frac{H_n^{(1)}(kb)\ \dot{J}_n(kb) - \dot{H}_n^{(1)}(kb)\ J_n(kb)}{n_0\ D_n^2\ H_n^{(1)}(kb) - p_r D_n^1\ \dot{H}_n^{(1)}(kb)}\ p_r P_n \qquad (3.18)$$

$$C_n = \frac{p_r D_n^1\ \dot{J}_n(kb) - n_o\ D_n^2\ J_n(kb)}{n_o\ D_n^2\ H_n^{(1)}(kb) - p_r D_n^1\ \dot{H}_n^{(1)}(kb)} \qquad (3.19)$$

where, $\dot{F}(z)$ implies the derivative of $F(z)$ with respect to the argument. For TM polarization:

$$D_n^1 = H_n^{(1)}(kn_0 b)\ H_n^{(2)}(kn_0 a) - H_n^{(2)}(kn_0 b)\ H_n^{(1)}(kn_0 a) \qquad (3.20a)$$

$$D_n^2 = \dot{H}_n^{(1)}(kn_o b)\ H_n^{(2)}(kn_o a) - \dot{H}_n^{(2)}(kn_o b)\ H_n^{(1)}(kn_o a) \qquad (3.20b)$$

$$P_n = H_n^{(2)}(kn_o a) \qquad (3.20c)$$

While, for TE polarization:

$$D_n^1 = H_n^{(1)}(kn_o b)\ \dot{H}_n^{(2)}(kn_o a) - H_n^{(2)}(kn_o b)\ \dot{H}_n^{(1)}(kn_o a) \qquad (3.21a)$$

$$D_n^2 = \dot{H}_n^{(1)}(kn_o b)\ \dot{H}_n^{(2)}(kn_o a) - \dot{H}_n^{(2)}(kn_o b)\ \dot{H}_n^{(1)}(kn_o a) \qquad (3.21b)$$

$$P_n = \dot{H}_n^{(2)}(kn_0 a) \qquad (3.21c)$$

It is possible to generate at least two equivalent expressions for the RCS based on the equations presented above. Having solved for the coefficients in the series expansions, Equation 3.16 can be substituted into Equation 3.1 directly or Equation 3.15 can be substituted into Equation 3.13 and the resulting integral expressions evaluated before substituting into Equation 3.1. The latter method will be used, even though it requires more work, because it generates a series expression for the RCS which is easily compared to an OSRC approximation.

Substituting the expressions for Φ^i and Φ^D into Equation 3.13 and evaluating the resulting integrals yields the following expression for the RCS.

$$\sigma = \frac{(\pi kb)^2}{k} \left| \sum_{n=0}^{n=\infty} \alpha_n E_n(n_o D_n^2 J_n(kb) - p_r D_n^1 \dot{J}_n(kb))\cos(n\Theta) \right|^2 \qquad (3.22a)$$

where, α_n is 1 for n = 0 and 2 otherwise and,

$$E_n = \frac{\dot{J}_n(kb) - \beta_n^E J_n(kb)}{p_r n_o D_n^2 - \beta_n^E D_n^1} \qquad (3.22b)$$

$$\beta_n^E = \dot{H}_n^{(1)}(kb) / H_n^{(1)}(kb) \qquad (3.22c)$$

and p_r, D_n^1, and D_n^2 are polarization dependent and are defined above.

OSRC Approximation for Circular Geometries

Two equivalent OSRC solutions will be derived. The first method produces a series expression for the RCS that is easily compared to the exact solution presented above. The other method shows how the OSRC solution for the dielectric coated cylinder is an extension of the OSRC solution for the perfectly conducting cylinder and is more amenable to numerical solutions for arbitrary geometries. All of the work presented here uses the second order boundary value operator used by Kriegsmann and others in their development of the OSRC approximation for the RCS of a perfectly conducting cylinder (Kriegsmann and others, 1987:155).

For Γ_1 a circle of radius a, Γ_2 a circle of radius b, where $b \geq a$, and using the far field approximations for the Green's function and its normal derivative presented above, Equation 3.10 can be reduced to:

$$\Phi_f^s = bG_0 \int_0^{2\pi} \left[\frac{\delta \Phi^s}{\delta r'} + jk\cos(\theta - \theta') \, \Phi^s \right] e^{-jkb\cos(\theta - \theta')} d\theta' \tag{3.23}$$

where Φ_f^s is the far field approximation for the scattered field and G_0 is defined in Equation 3.12c.

The first OSRC method uses the boundary conditions to substitute for the scattered field and its derivative in the integrand of Equation 3.23 in terms of the incident field and the field in the dielectric material. Then the OSRC

operator is used, instead of the Sommerfeld radiation conditions, to find an approximation for the field in the dielectric material. The resulting integrals are evaluated and the final expression substituted into Equation 3.1. This method is very similar to the procedure presented above for the exact solution and produces a series expression for the RCS which is almost identical to Equation 3.22.

The second method uses the OSRC operator to find an approximate expression for the normal derivative of the scattered field in the integrand of Equation 3.23 and for the field in the dielectric material. The boundary conditions are used to substitute for the scattered field on the surface of the dielectric material and the resulting integrals are evaluated to find the far field approximation for the scattered field. The expression for the RCS is found by substituting into Equation 3.1. This method produces a solution which, for the special case of a = b, can be easily shown to reduce to the OSRC approximation for the RCS of a perfectly conducting cylinder published by Kriegsmann and others (Kriegsmann and others, 1987:156). Since both methods use the OSRC approximation for the field in the dielectric material, the details of this derivation will be presented first.

The assumed form for Φ^D and the boundary condition on Γ_1 remain the same as for the exact solution. Therefore, Φ^D

can be expressed as a summation of eigenfunctions with one unknown coefficient.

$$\Phi^D = \sum_{n=-\infty}^{n=\infty} j^n A_n \left[H_n^{(1)}(kn_o r) - B_n H_n^{(2)}(kn_o r) \right] e^{jn\theta} \qquad (3.24a)$$

where,

$$B_n = \frac{H_n^{(1)}(kn_0 a)}{H_n^{(2)}(kn_0 a)} \qquad \text{for TM polarization} \qquad (3.24b)$$

or,

$$B_n = \frac{\dot{H}_n^{(1)}(kn_o a)}{\dot{H}_n^{(2)}(kn_o a)} \qquad \text{for TE polarization} \qquad (3.24c)$$

and A_n is the unknown coefficient. A_n is found by using an n^{th} order OSRC boundary operator and the boundary conditions on Γ_2.

The n^{th} order OSRC boundary operator, B_n, is used in lieu of the Sommerfeld radiation condition by imposing the following condition on the solution:

$$B_n\{ \Phi^s \} = 0 \quad \text{on } \Gamma_2 \qquad (3.25)$$

Equation 3.25 is an approximation with an error term that is proportional to $r^{(-2n-1/2)}$, where r is the distance from the origin to the surface of the dielectric material and n is the order of the operator. Appendix A explains the motivation for using this approximation and presents a derivation of the error term and the second order operator.

The second order OSRC operator is (Kriegsmann, 1987:155):

$$B_2 = \frac{\delta}{\delta r} + \frac{1}{2r} - jk - \frac{\frac{\delta^2}{\delta\theta^2} - \frac{1}{4}}{2r\,(1 - jkr)} \qquad (3.26)$$

Substituting Equation 3.26 into Equation 3.25 and rearranging terms yields:

$$\frac{\delta\Phi^s}{\delta r} = k\,\hat{B}\,\{\,\Phi^s\,\} \quad \text{on } \Gamma_2 \qquad (3.27a)$$

where,

$$\hat{B} = j - \frac{1}{2kr} + \frac{\frac{\delta^2}{\delta\theta^2} - \frac{1}{4}}{2kr(1 - jkr)} \qquad (3.27b)$$

Rearranging the boundary conditions by solving Equations 3.8b and 3.8c or Equations 3.9b and 3.9c for the scattered field and its derivative and substituting the resulting expressions into Equation 3.27a yields:

$$\frac{1}{p_r}\frac{\delta\Phi^D}{\delta r} - k\hat{B}\,\{\,\Phi^D\,\} = \frac{\delta\Phi^i}{\delta r} - k\hat{B}\,\{\,\Phi^i\,\} \qquad (3.28)$$

where p_r is μ_r for incident TM polarization or ϵ_r for TE polarization. Substituting the assumed form for Φ^D and Φ^i, multiplying both sides of Equation 3.28 by $\exp(-jm\theta)$ and integrating from 0 to 2π yields the unknown coefficient A_n:

$$A_n = \frac{\dot{J}_n(kb) - \beta_n^o J(kb)}{n_o D_n^2 - p_r \beta_n^o D_n^1}\; p_r P_n \qquad (3.29a)$$

where D_n^1, D_n^2, p_r and P_n are polarization dependent and

defined above in Equations 3.20 and 3.21 and:

$$\beta_n^o = j - \frac{1}{2kr} - \frac{n^2 - 1/4}{2kr(1 - jkr)} \qquad (3.29b)$$

Now that the OSRC approximation for the field in the dielectric layer is known, the approximations for the scattered field can be found using the two methods described above.

Using the boundary conditions to substitute for the scattered field and its derivative in the integrand of Equation 3.23 yields:

$$\Phi_f^s = bG_0 \int_0^{2\pi} [\frac{1}{p_r} \frac{\delta \Phi^D}{\delta r'} + jk\cos(\theta - \theta') \Phi^D] e^{-jkb\cos(\theta - \theta')} d\theta'$$

$$- bG_0 \int_0^{2\pi} [\frac{\delta \Phi^i}{\delta r'} + jk\cos(\theta - \theta') \Phi^i] e^{-jkb\cos(\theta - \theta')} d\theta' \qquad (3.30)$$

which is identical to Equation 3.13 above. The two terms in the second integral of Equation 3.30 cancel; therefore, its contribution is zero. Substituting the expression for Φ^D in the first integral yields:

$$\Phi_f^s = kbG_0 \sum_{n=-\infty}^{n=\infty} j^n E_n \; I \qquad (3.31a)$$

where,

$$I = \int_0^{2\pi} [n_o D_n^2 + j p_r D_n^1 \cos(\theta - \theta')] e^{jn\theta' - jkb\cos(\theta - \theta')} d\theta' \qquad (3.31b)$$

The integral in equation 3.31 is evaluated using the following Bessel function identities.

$$2\pi j^{-n} e^{jn\theta} J_n(z) = \int_0^{2\pi} e^{jn\theta' - jz\cos(\theta - \theta')} d\theta' \qquad (3.32)$$

and

$$j\, 2\pi j^{-n} e^{jn\theta} \dot{J}_n(z) = \int_0^{2\pi} \cos(\theta - \theta')\, e^{jn\theta' - jz\cos(\theta - \theta')} d\theta' \qquad (3.33)$$

Substituting Equations 3.32 and 3.33 into Equation 3.31 yields the OSRC approximation for the scattered field.

$$\Phi_f^s = 2\pi kbG_0 \sum_{n=-\infty}^{n=\infty} A_n \left[n_o D_n^2 J_n(kb) - p_r D_n^1 \dot{J}_n(kb) \right] e^{jn\theta} \qquad (3.34)$$

Substituting into Equation 3.1 yields the OSRC approximation for the RCS using the first method.

$$\hat{\sigma}_1 = \frac{(\pi kb)^2}{k} \left| \sum_{n=0}^{n=\infty} \alpha_n A_n \left(n_o D_n^2 J_n(kb) - p_r D_n^1 \dot{J}_n(kb) \right) \cos(n\theta) \right|^2 \qquad (3.35)$$

where α_n is 1 for n = 0 and 2 otherwise. A thorough comparison of this approximation and the exact solution is presented below.

The second method uses the OSRC boundary operator and the boundary condition $\Phi^s = \Phi^D - \Phi^i$ on the surface of the dielectric layer regardless of polarization to find a substitution for the derivative of the scattered field in the integrand of Equation 3.23.

$$\frac{\delta \Phi^s}{\delta r} = k \hat{B} \{ \Phi^s \} = k \hat{B} \{ \Phi^D - \Phi^i \} \quad \text{on } \Gamma_2 \qquad (3.36)$$

Substituting Equation 3.36 and the boundary condition mentioned above into Equation 3.23 yields:

$$\Phi_f^s = kbG_0 (I_1 - I_2) \qquad (3.37a)$$

where,

$$I_1 = \int_0^{2\pi} [\hat{B}\{ \Phi^D \} + j\cos(\theta - \theta') \Phi^D] e^{-jkbcos(\theta - \theta')} d\theta' \qquad (3.37b)$$

$$I_2 = \int_0^{2\pi} [\hat{B}\{ \Phi^i \} + j\cos(\theta - \theta') \Phi^i] e^{-jkbcos(\theta - \theta')} d\theta' \qquad (3.37c)$$

Using the series expression for Φ^D and the exponential expression for Φ^i in the argument of the $\hat{B}$ operator yields:

$$\hat{B}\{ \Phi^D \} = \sum_{n=-\infty}^{n=\infty} j^n A_n D_n^1 \beta_n^0 e^{jn\theta} \quad \text{on } \Gamma_2 \qquad (3.38a)$$

$$\hat{B}\{ \Phi^i \} = (j - \frac{1}{2kb} + \frac{1}{8kb(1 - jkb)} - \frac{jkbcos\theta + (kbsin\theta)^2}{2kb(1 - jkb)}) e^{jkbcos\theta} \qquad (3.38b)$$

Using Equation 3.38a,

$$I_1 = \sum_{n=-\infty}^{n=\infty} j^n A_n D_n^1 (\int_0^{2\pi} [\beta_n^0 + j\cos(\theta - \theta')] e^{jn\theta' - jkbcos(\theta - \theta')} d\theta' \qquad (3.39)$$

Which is easily evaluated using Equations 3.32 and 3.32 to give:

$$I_1 = 2\pi \sum_{n=-\infty}^{n=\infty} A_n D_n^1 (\beta_n^o J_n(kb) - \dot{J}_n(kb)) e^{jn\theta} = -2\pi \sum_{n=-\infty}^{n=\infty} p_r E_n D_n^1 e^{jn\theta} \tag{3.40a}$$

where,

$$E_n = \frac{[\ \dot{J}_n(kb) - \beta_n^o J_n(kb)\ ]^2}{n_o D_n^2 - p_r \beta_n^o D_n^1} \tag{3.40b}$$

Evaluating I_2 required a little more work. Substituting Equation 3.38b into 3.37c yields:

$$I_2 = [j - \frac{1}{2kb} + \frac{1}{8kb(1-jkb)}] \int_0^{2\pi} e^{jkb(\cos\theta' - \cos(\theta - \theta'))} d\theta'$$

$$- \frac{jkb}{2kb(1 - jkb)} \int_0^{2\pi} \cos\theta' \ e^{jkb(\cos\theta' - \cos(\theta - \theta'))} d\theta'$$

$$- \frac{(kb)^2}{4kb(1 - jkb)} \int_0^{2\pi} (1 - \cos(2\theta'))\ e^{jkb(\cos\theta' - \cos(\theta - \theta'))} d\theta'$$

$$+ j \int_0^{2\pi} \cos(\theta - \theta')\ e^{jkb(\cos\theta' - \cos(\theta - \theta'))} d\theta' \tag{3.41}$$

Where the identity $\sin^2\theta = (\ 1 - \cos(2\theta)\ )/2$ has been used. Using the results of a good integral table (Gradshetyn and Ryzhik, 1980:482) and combining terms, Equation 3.41 reduces to:

$$I_2 = 2\pi\ [\ K_0\ J_0(z) + K_1\ \sin(\theta/2)\ J_1(z) + K_2\ \cos\theta\ \ J_2(z)] \tag{3.42a}$$

where $z = 2kb\sin(\theta/2)$ and

$$K_0 = j - \frac{1}{2kb} - \frac{kb}{4(1 - jkb)} + \frac{1}{8kb(1-jkb)} \qquad (3.42b)$$

$$K_1 = 1 + \frac{1}{2(1 - jkb)} \qquad (3.42c)$$

$$K_2 = \frac{kb}{4(1 - jkb)} \qquad (3.42d)$$

Using Equations 3.40 and 3.42 the final result for the OSRC approximation for the scattered field using the second method is:

$$\Phi_f^s = -2\pi kbG_0 \left[K_0 J_0(z) + K_1 \sin(\theta/2) J_1(z) + K_2 \cos\theta J_2(z) + p_r \sum_{n=-\infty}^{n=\infty} E_n D_n^1 e^{jn\theta} \right] \qquad (3.43)$$

Substituting equation 3.43 into Equation 3.1 yields the final expression for the RCS:

$$\hat{\sigma}_2 = \frac{(\pi kb)^2}{k} \left| K_0 J_0(z) + K_1 \sin(\theta/2) J_1(z) + K_2 \cos\theta J_2(z) + p_r \sum_{n=0}^{n=\infty} \alpha_n E_n D_n^1 \cos(n\theta) \right|^2 \qquad (3.44)$$

In order to show that Equation 3.44 reduces to the OSRC approximation for the RCS of a conducting cylinder for the special case of a = b and incident TM polarization, it is necessary to show that the summation goes to zero and to make a high frequency approximation for the K_i terms. For a = b and incident TM polarization, $D_n^1 = 0$ for all n and every term in the summation in Equation 3.44 is identically zero. The high frequency approximation for the K_i terms is:

$$\frac{1}{(1-jkb)} \approx \frac{j}{kb}$$

and ignoring terms that are proportional to $(kb)^{-2}$, The expressions for the K_i terms reduce to:

$$K_0 = j - \frac{1}{2kb} - \frac{j}{4} \tag{3.45a}$$

$$K_1 = 1 + \frac{j}{2kb} \tag{3.45b}$$

$$K_2 = \frac{j}{4} \tag{3.45c}$$

Using the Bessel function identity:

$$J_2(z) = (2/z)J_1(z) - J_0(z)$$

and the trigonometry identity $1 + \cos\theta = 2\cos^2\theta$, the expression for the RCS reduces to:

$$\hat{\sigma}_3 = \frac{(\pi kb)^2}{k} \left| \left[j - \frac{1}{2kb} - \frac{j}{2}\cos^2(\theta) \right] J_0(z) + G\, J_1(z) \right|^2 \tag{3.46a}$$

$$G = [1 + j/(2kb)] \sin(\theta/2) + \cos(\theta)/2z \tag{3.46b}$$

Equation 3.46 is identical to the OSRC approximation for the RCS of a conducting cylinder published by Kriegsmann and others (Kriegsmann and others, 1987:156).

Comparison of the OSRC and Exact Solutions

Two expressions comparing the OSRC solution using the first method and the exact solution were derived. The first expression shows how the OSRC solution converges to the exact solution as kb gets large. The second expression shows

how the properties of the dielectric layer play a large role in determining the overall accuracy of the OSRC solution.

Comparing Equation 3.22 to Equation 3.35, the only difference occurs for the β_n terms in the coefficients E_n and A_n. Repeating the definition of these terms:

$$\beta_n^O = j - \frac{1}{2kr} - \frac{n^2 - 1/4}{2kr(1 - jkr)} \qquad (3.29b)$$

for the OSRC solution and,

$$\beta_n^E = \dot{H}_n^{(1)}(kb) \; / \; H_n^{(1)}(kb) \qquad (3.23b)$$

for the exact solution. Using the asymptotic expansions for the Hankel function and its derivative (Abromowitz and Stegun, 1972:364-365) the first four terms in the ratio of Equation 3.23b are:

$$\frac{\dot{H}^{(1)}(kb)}{H_n^{(1)}(kb)} = j - \frac{1}{2kb} + j\,\frac{1 - 4n^2}{8(kb)^2} + \frac{1 - 4n^2}{8(kb)^3} + O(kb)^{-4} \qquad (3.47)$$

Rewriting the last term in Equation 3.23b as a converging geometric series:

$$\beta_n^O = j - \frac{1}{2kb} + \frac{1 - 4n^2}{8(kb)^2}\left[\, j + \frac{1}{kb} - \frac{j}{(kb)^2} - \frac{1}{(kb)^3} + \ldots \,\right] \qquad (3.48)$$

Comparison of Equations 3.47 and 3.48 shows that the OSRC approximation should converge to the exact solution as kb gets large. This convergence should occur fairly quickly since the two series agree to at least order three.

However, the overall accuracy of the OSRC technique is determined by the difference between each coefficient in the two series solutions. Letting the exact solution be represented as:

$$\sigma = \frac{(\pi kb)^2}{k} \left| \sum_{n=0}^{n=\infty} \alpha_n F_n^E \cos(n\theta) \right|^2 \qquad (3.49)$$

and the OSRC solution as:

$$\hat{\sigma}_1 = \frac{(\pi kb)^2}{k} \left| \sum_{n=0}^{n=\infty} \alpha_n F_n^O \cos(n\theta) \right|^2 \qquad (3.50)$$

then the accuracy of the OSRC technique is determined by how closely F_n^O approximates F_n^E for all n in which the magnitude of F_n^E is significant. In order to derive an expression which relates F_n^O to F_n^E, let:

$$\beta_n^O - \beta_n^E = e_n \quad \text{and} \quad F_n^E = N_n^E / D_n^E$$

Then F_n^O can be written as:

$$F_n^O = [n_o D_n^2 J_n(kb) - p_r D_n^1 \dot{J}_n(kb)] \quad \frac{\dot{J}_n(kb) - \beta_n^E J_n(kb) + e_n J_n(kb)}{n_o D_n^2 - p_r \beta_n^E D_n^1 + p_r e_n D_n^1} \qquad (3.51)$$

Rearranging terms, Equation 3.51 becomes:

$$F_n^O = \frac{N_n^E + [n_o D_n^2 J_n(kb) - p_r D_n^1 \dot{J}_n(kb)] e_n J_n(kb)}{D_n^E + p_r e_n D_n^1} \qquad (3.52)$$

After some manipulation, equation 3.52 can be rearranged as:

$$F_n^O = F_n^E \{1 + e_n(1 + Y_n) (1 - X_n + X_n^2 - . . .)\} \quad (3.53a)$$

where,

$$Y_n = \frac{[n_o D_n^2 J_n(kb) - p_r D_n^1 \dot{J}_n(kb)] \beta_n \dot{J}_n(kb) - p_r D_n^1 F_n^E}{[n_o D_n^2 J_n(kb) - p_r D_n^1 \dot{J}_n(kb)] [J_n(kb) - \beta_n^E \dot{J}_n(kb)]} \quad (3.53b)$$

$$X_n = \frac{e_n p_r D_n^1}{n_o D_n^2 - p_r \beta_n^E D_n^1} \quad (3.53c)$$

Due to the complexity of the Y_n and X_n terms in Equation 3.53, it is extremely difficult to predict how closely F_n^O approximates F_n^E. However, if both Y_n and X_n are much less than one, then the OSRC technique should produce a good approximation for the RCS for even small values of kb. The dielectric material parameters ϵ_r, u_r, σ and the thickness of the dielectric layer should have a significant effect on the accuracy of the OSRC solution.

Summary

The RCS of a circular cylinder coated with a lossy dielectric and/or magnetic material was derived using the method of eigenfunction expansion and the OSRC approximation technique for both incident polarizations. Two equivalent OSRC solutions were derived. One was shown to reduce to the

OSRC approximation for the RCS of a conducting cylinder alone as the thickness of the dielectric material went to zero. The other OSRC solution was compared to the eigenfunction solution. The OSRC solution and the eigenfunction solution were nearly identical; however, the overall accuracy of the OSRC technique was shown to be goverened by a complicated expression which was dependent on the dielectric material parameters as well as the kb product.

IV. Results

Introduction

Nine computer programs were written to compare the OSRC solutions to the eigenfunction solution for three different circumstances. One set of programs computes the monostatic RCS for fixed frequency and conductor radius and increasing dielectric coating radius. Another set of programs computes the monostatic RCS for fixed geometry and variable frequency. The last set of programs computes the bistatic RCS for fixed geometry and frequency for $0 \leq \Theta \leq \pi$ radians. Each set of programs consists of one program to compute the eigenfunction solution and two programs to compute the two OSRC solutions presented in Chapter 3. Both OSRC programs produced identical results, within the limits of the graphs, for all of the data presented below. Therefore, only one OSRC plot appears on each of the figures. A listing of the programs is provided in Appendix C. All of the programs use a common set of subroutines to evaluate the necessary Bessel functions. A complete description of the algorithms and a listing of the subroutines is provided in Appendix B. For all of the programs the summation loops were stopped whenever the magnitude of the coefficient just computed was five orders of magnitude less than the magnitude of the sum.

The programs accept complex valued ϵ_r and μ_r and a non zero conductivity σ.

In order to limit the amount of data presented, a few cases were chosen that were representative of the general trends observed. For the fixed frequency and variable thickness programs, a conductor radius of 0.25 wavelengths and 1 wavelength for k = 200 (ka = 1.57 or ka = 6.28) was chosen as the baseline for comparison for both polarizations. The values chosen for the real part of the dielectric material parameters, ϵ_r and μ_r, remained the same at 2.54 and 1.0, respectively, for all the data. The values chosen for the imaginary part of the relative permittivity were 0.0, 0.25, 1.0 and in some cases 1.5. The imaginary part of the relative permeability was left at 0.0. For the fixed geometry and variable frequency programs, the kb product was varied from 0.06 to 7.1 for b = 3a and from 0.17 to 20.5 for b = 8.5a for both polarizations. The dielectric material parameters were varied as in the variable thickness case described above. In addition to the variable thickness and variable frequency cases, several representative sets of input parameters were chosen for the bistatic RCS computations. The conductivity was set to zero for all the data.

A non-zero imaginary part of either the relative permittivity or permeability implies the material absorbs

power from the field. For this reason, the case where the imaginary part of ϵ_r was zero was called the lossless case; 0.25 was called the slightly lossy case; 1.0 was called the lossy case and 1.5 was called the very lossy case.

The above parameters were chosen because they illustrate how the OSRC solution converges to the eigenfunction solution as the kb product or the material parameters vary. The goal here is to determine the ranges of validity of the OSRC technique, not to model a specific dielectric coating. The OSRC approximation was said to agree well with the exact solution whenever the difference between the two solutions was less than 2 db.

First the variable thickness data will be presented, followed by the variable frequency data and then the bistatic data. A brief summary of the pertinent features of each data set is included with the data. A complete analysis of all the data is included following the bistatic data.

Variable Thickness Data

Figures 4 through 6 are plots of the RCS versus kb for the lossless, slightly lossy and lossy cases for ka = 1.57 and incident TM polarization. Figures 7 through 9 are the same data for incident TE polarization and Figure 10 is the very lossy data. For all of these cases, the OSRC solution

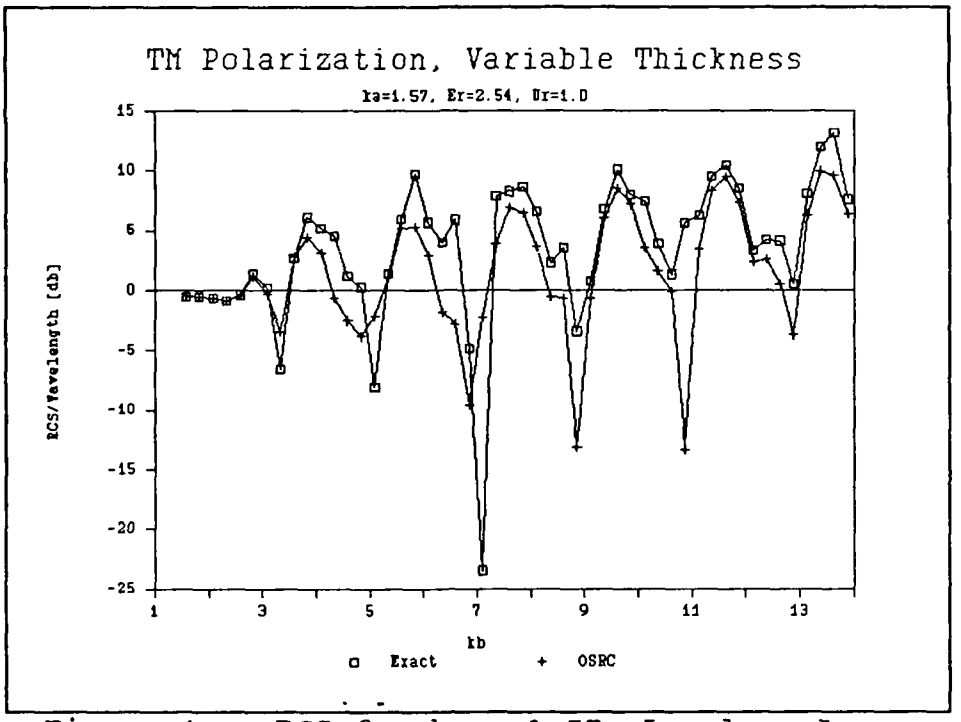

Figure 4. RCS for ka = 1.57, Lossless Layer

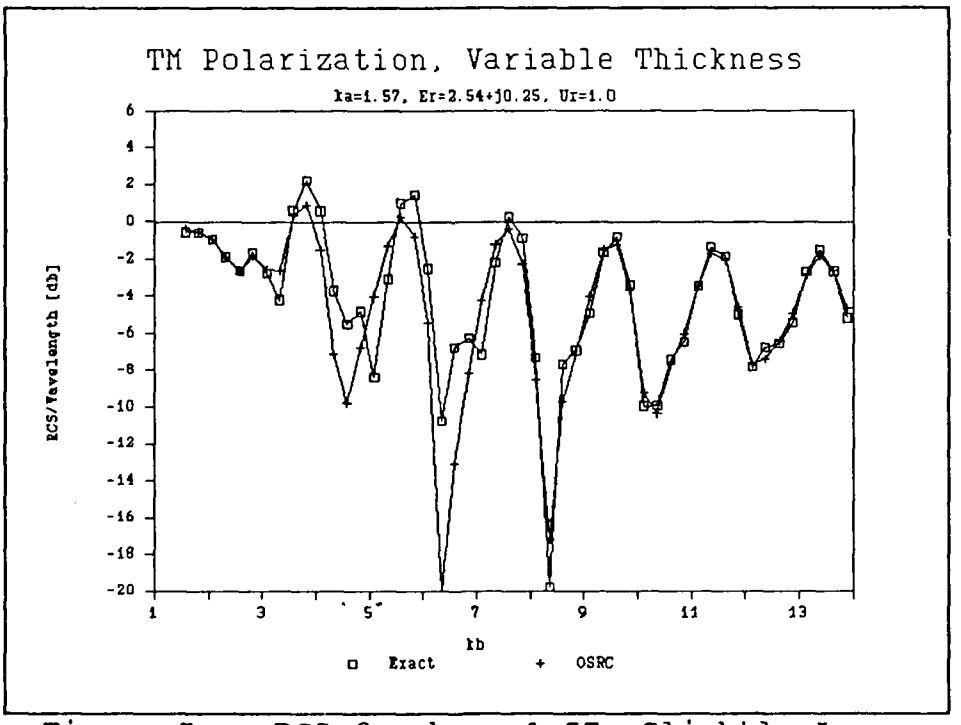

Figure 5. RCS for ka = 1.57, Slightly Lossy Layer

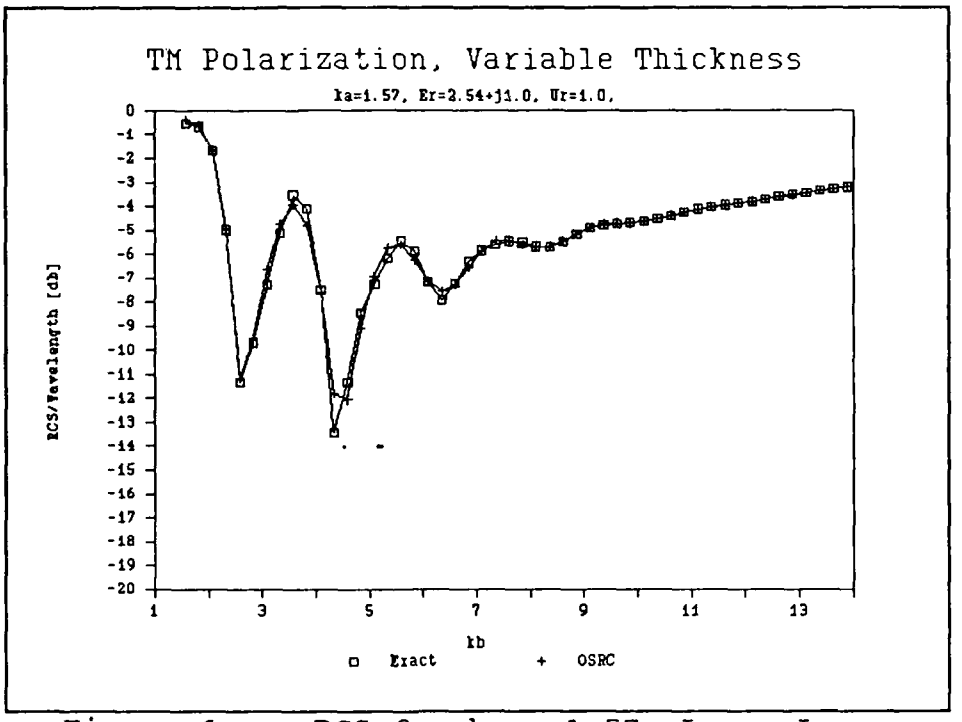

Figure 6. RCS for ka = 1.57, Lossy Layer

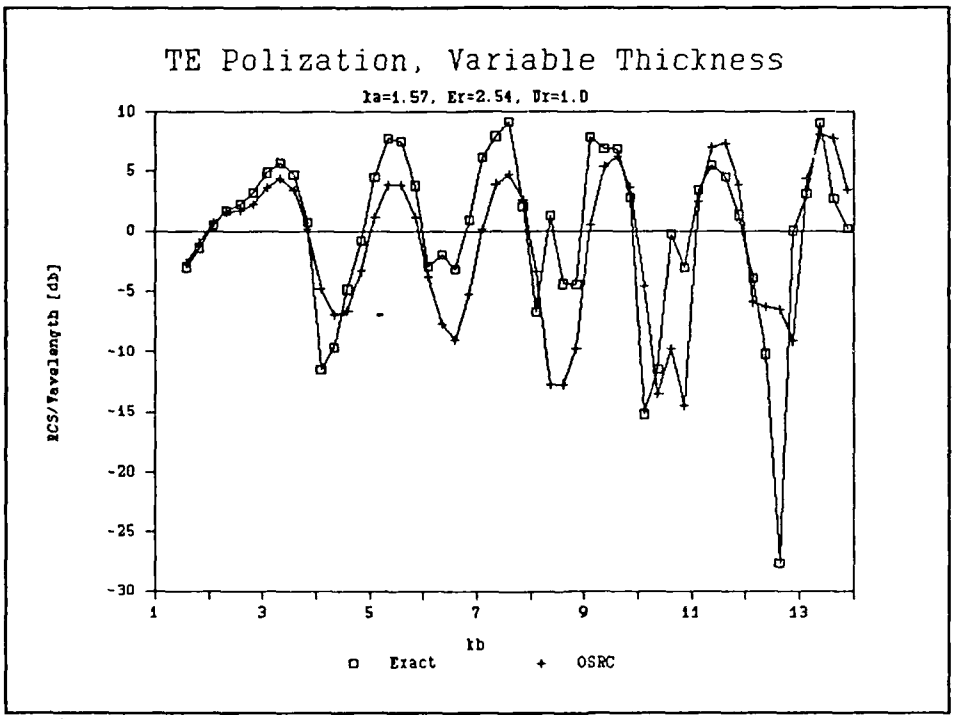

Figure 7. RCS for ka = 1.57, Lossless Layer

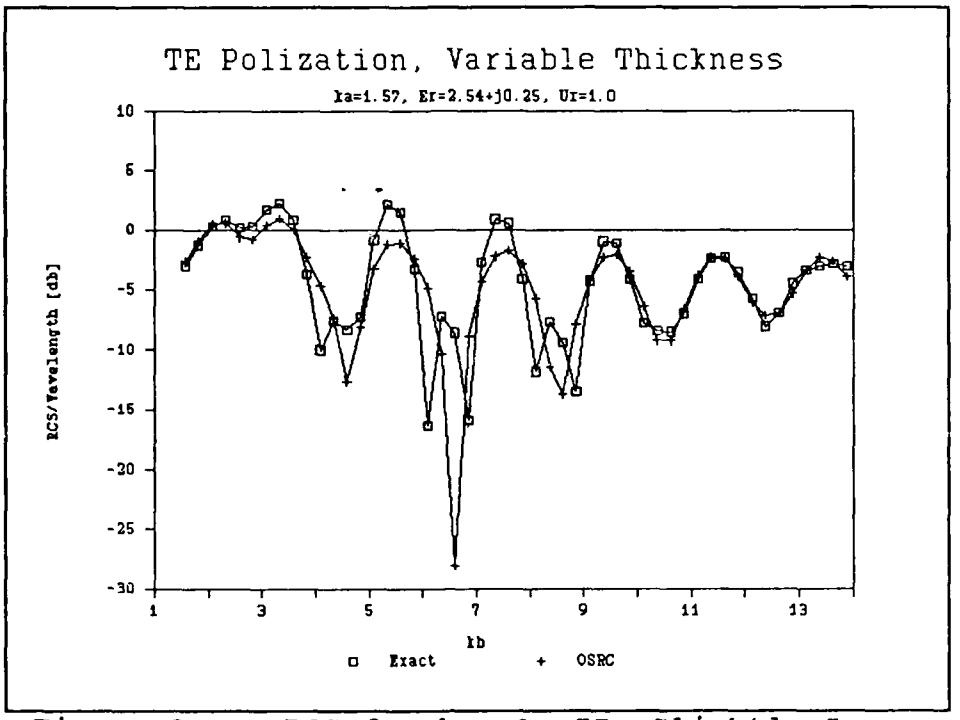

Figure 8. RCS for ka =1 .57, Slightly Lossy Layer

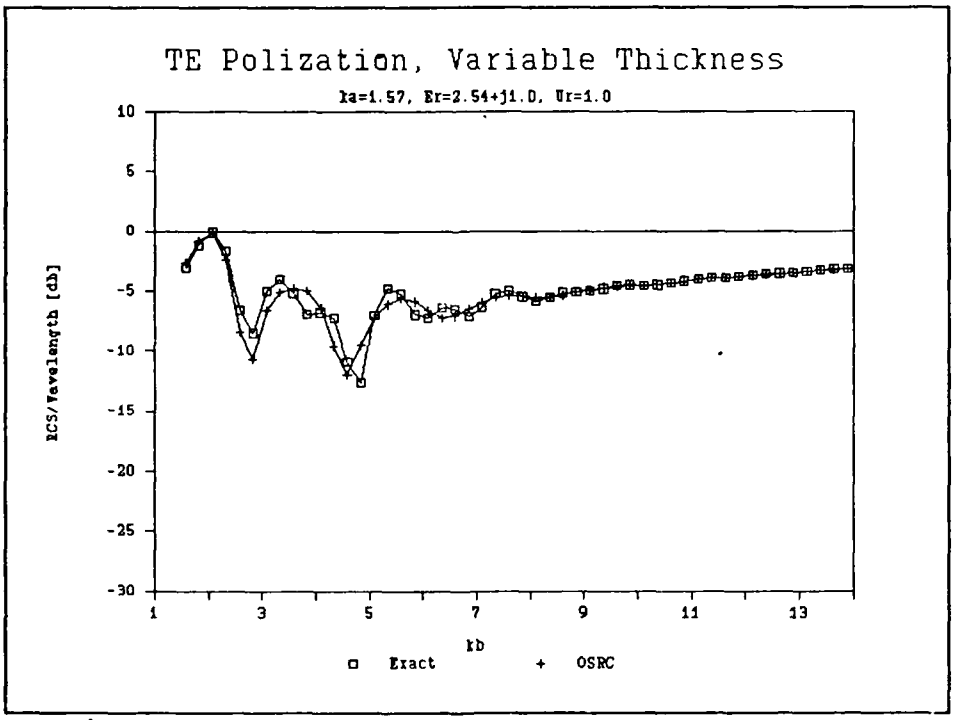

Figure 9. RCS for ka = 1.57, Lossy Layer

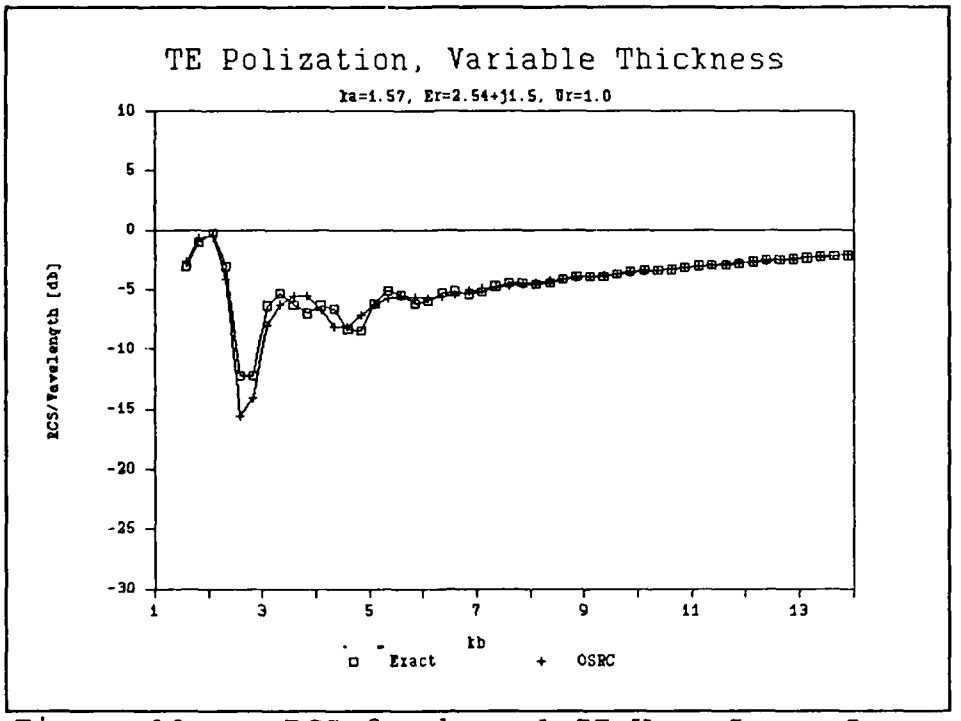

Figure 10. RCS for ka = 1.57 Very Lossy Layer

agreed well with the eigenfunction (exact) solution for kb less than approximately 3.0. This is equivalent to the thickness of the dielectric layer less than one-half wavelength. When the thickness exceeded one-half wavelength, the OSRC solution agreed with the exact solution for certain combinations of loss and kb only. For incidentTM polarization and the imaginary part of the relative permittivity equal to 0.25, Figure 5, the kb product had to be greater than 7.2 for the two solutions to agree. For the lossy case, Figure 6, the two solutions

agreed for all values of kb. For incident TE polarization and the imaginary part of the relative permittivity equal to 0.25, Figure 8, kb had to be greater than 8 for the two solutions to agree. For the lossy case, Figure 9, the kb had to be greater than 7.0 for the two solutions to agree. For the very lossy case, Figure 10, the two solutions agreed for all values of kb.

Figures 11 and 12 are plots of the RCS versus kb for the lossless and slightly lossy cases and ka = 6.28 for incident TM polarization. For the lossless case, Figure 11, the OSRC solution agreed well with the exact solution for kb less than approximately 7.5. This is equivalent to the thickness of the dielectric layer less than 0.2 wavelengths. For the kb product greater than 14, the two solutions agreed everywhere except at nulls. For the slightly lossy case, Figure 12, the OSRC solution was within 2 db of the exact solution for all values of kb.

Figures 13 through 15 are the data for incident TE polarization. For the lossless dielectric case, Figure 13, there was virtually no region where the OSRC solution agreed well with the eigenfunction solution. For the slightly lossy case, Figure 14, The two solutions agreed whenever kb was greater than 8 and for the ossy case, Figure 15, the two solutions agreed for all values of kb.

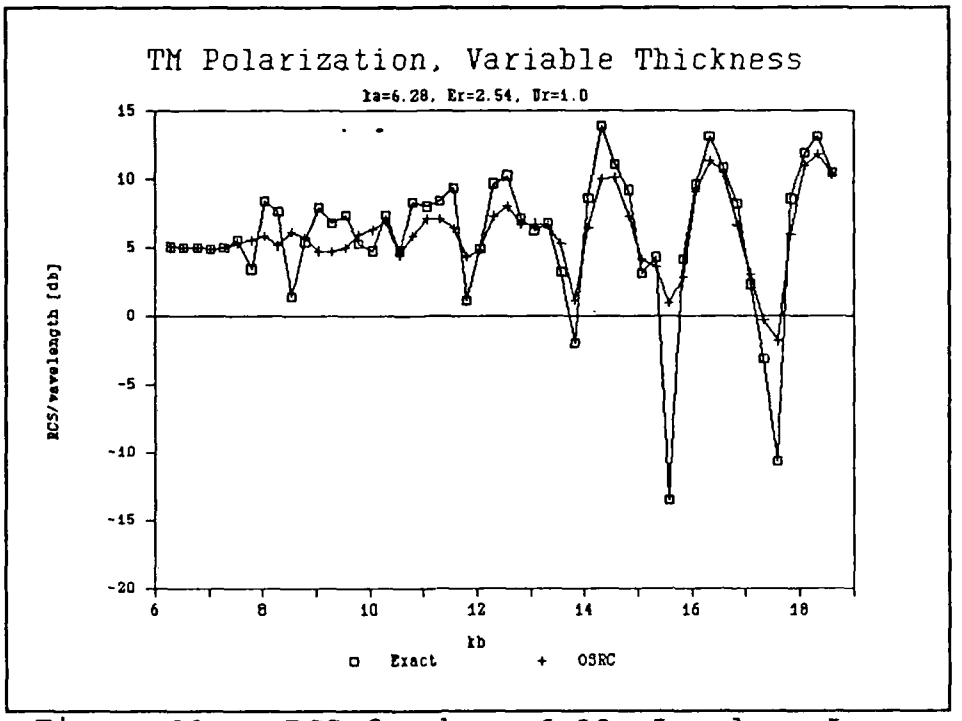

Figure 11. RCS for ka = 6.28, Lossless Layer

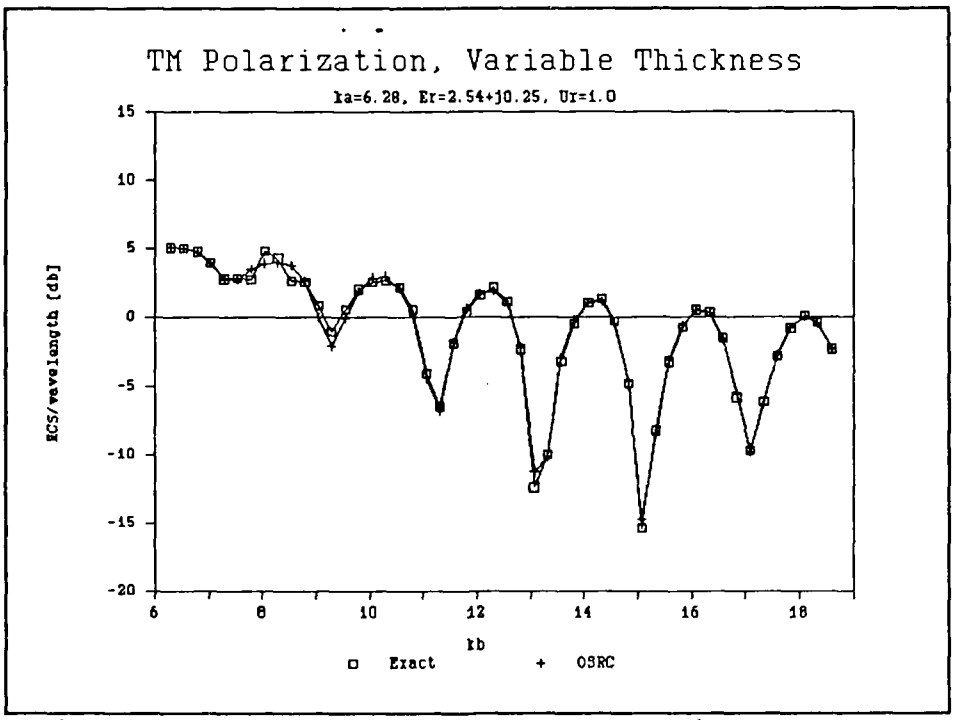

Figure 12. RCS for ka = 6.28 Slightly Lossy Layer

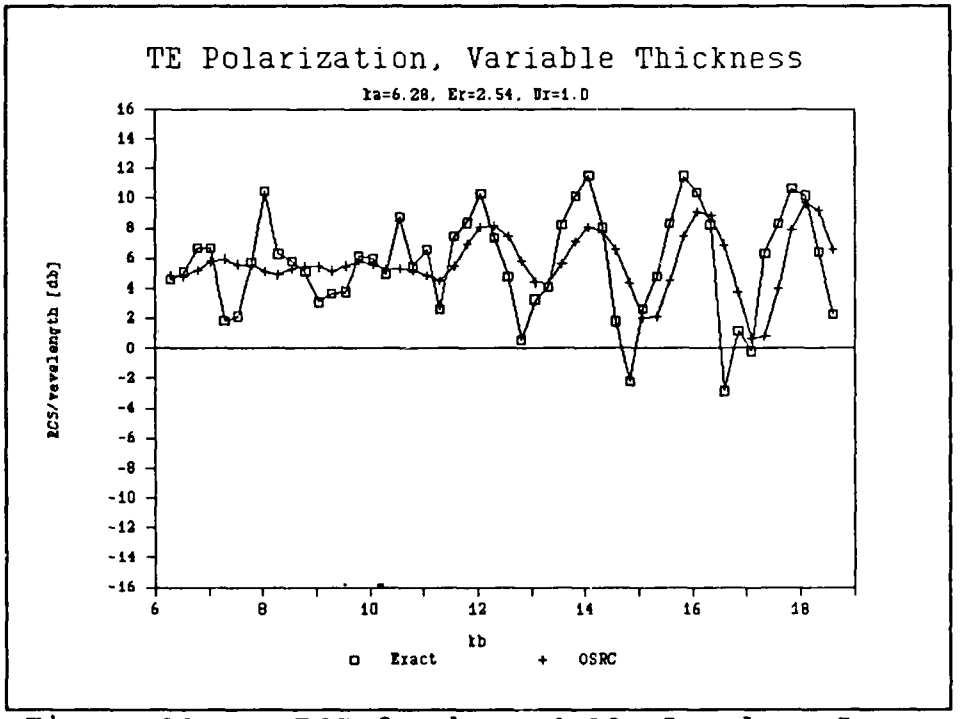

Figure 13. RCS for ka = 6.28, Lossless Layer

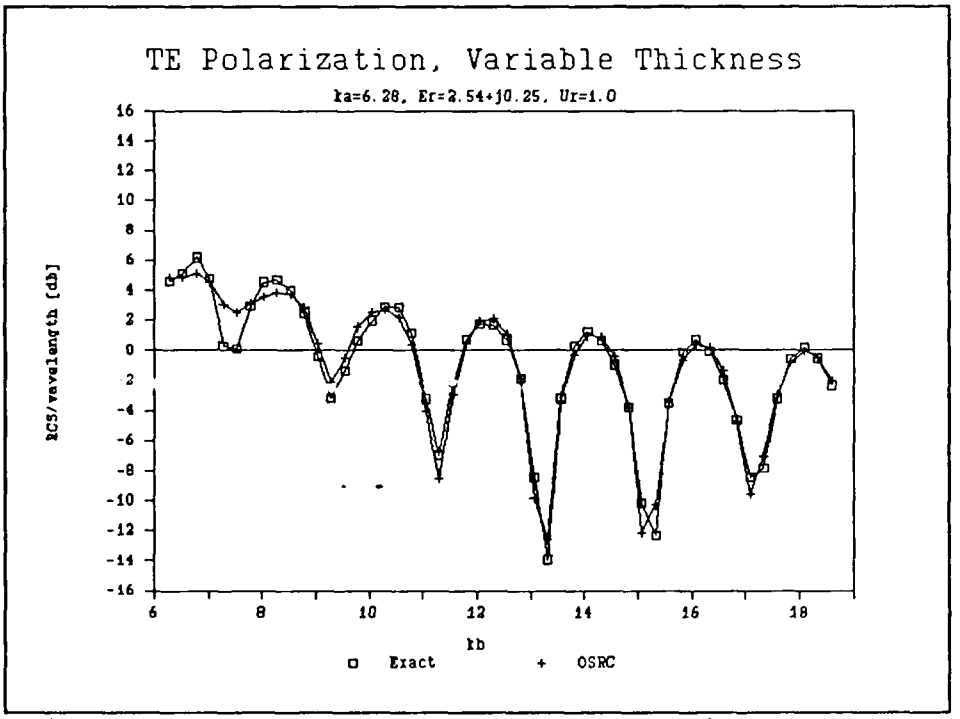

Figure 14. RCS for ka = 6.28, Slightly Lossy layer

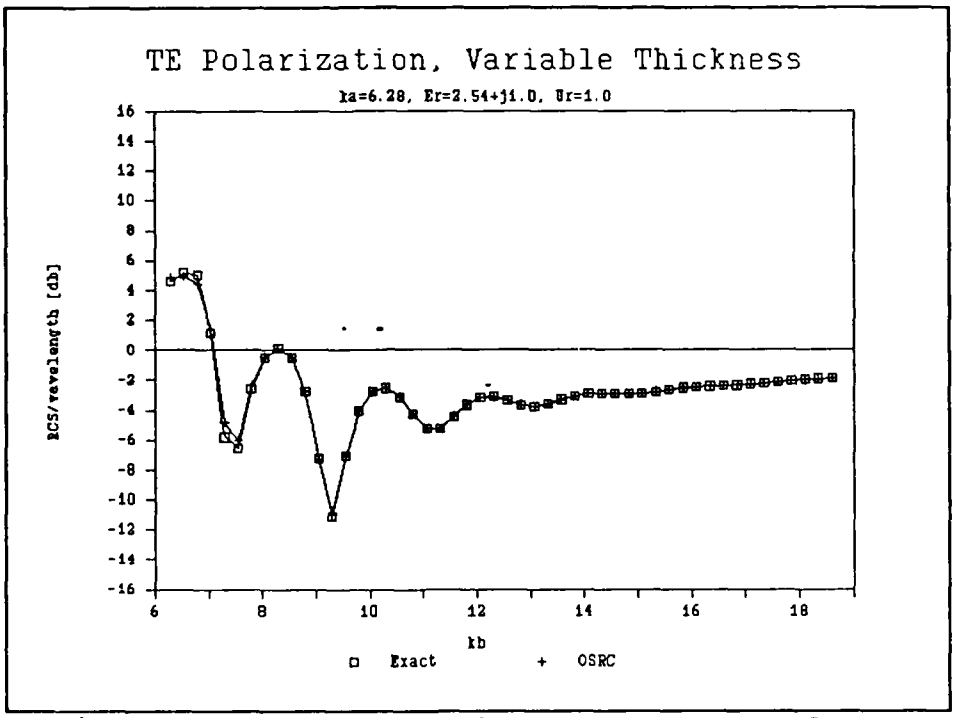

Figure 15. RCS for ka = 6.28, Lossy layer

Variable Frequency Data

Figures 16 through 18 are the data for the lossless, slightly lossy and lossy cases for b = 3a and increasingfrequency for incident TM polarization. Figure 19 through 21 are the same data for incident TE polarization. Figure 22 is the data for the very lossy case and incident TE polarization. The radius of the conducting cylinder, a, varies from 0.003 wavelengths to 0.4 wavelengths as k is increased from 10 to 1210. For the thickness of the coating less than approximately 0.4 wavelengths (kb < 3.6), the two solutions agreed well for both polarizations. For higher

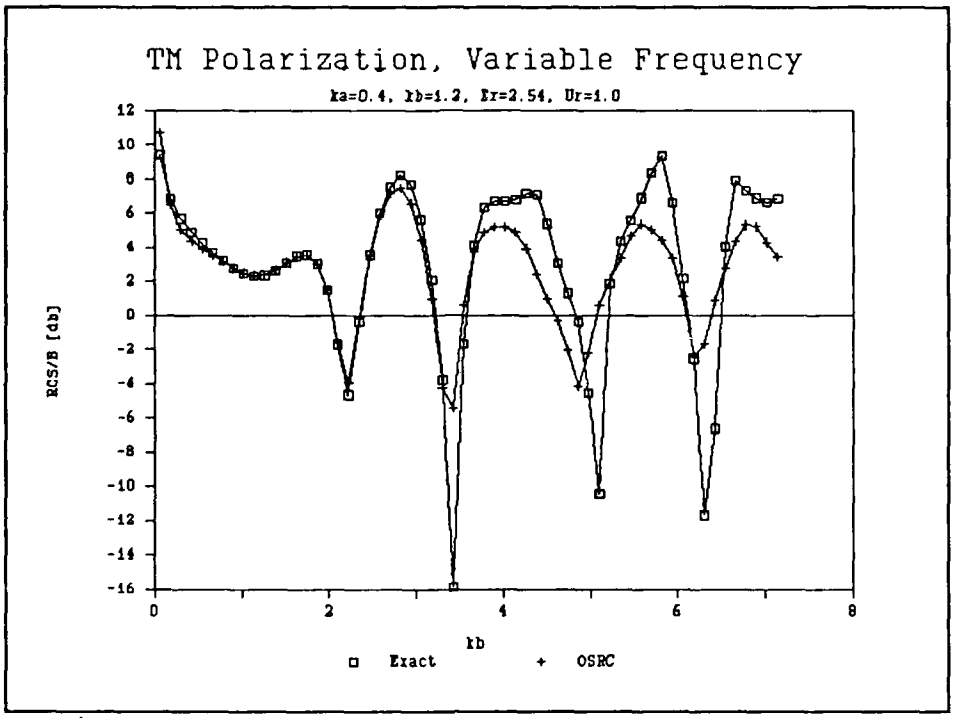

Figure 16. RCS for b = 3a, Lossless Layer

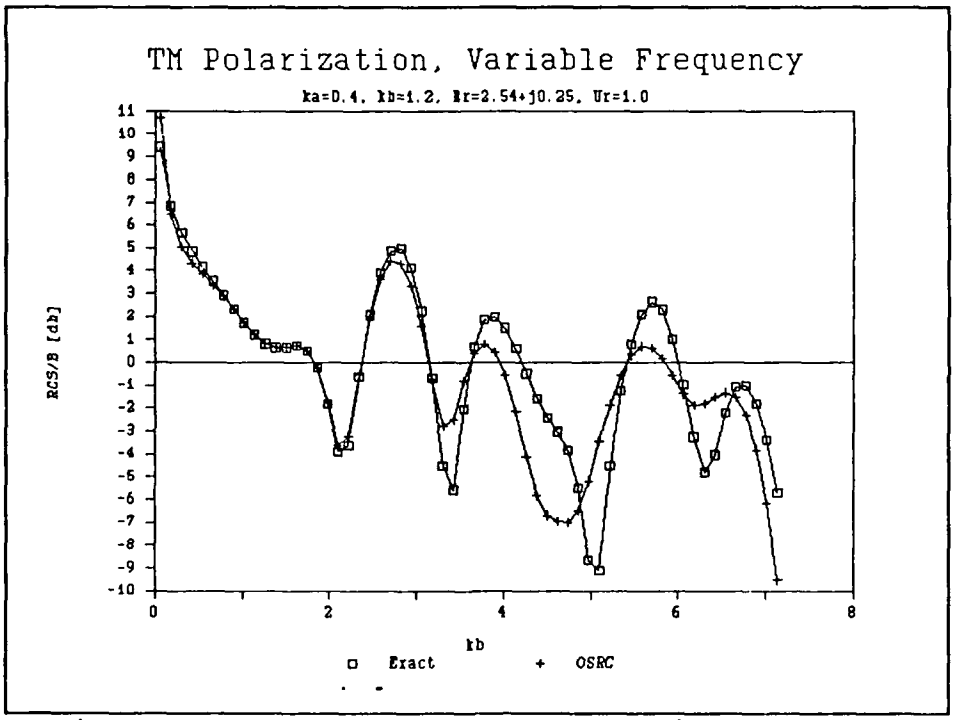

Figure 17. RCS for b = 3a, Slightly Lossy Layer

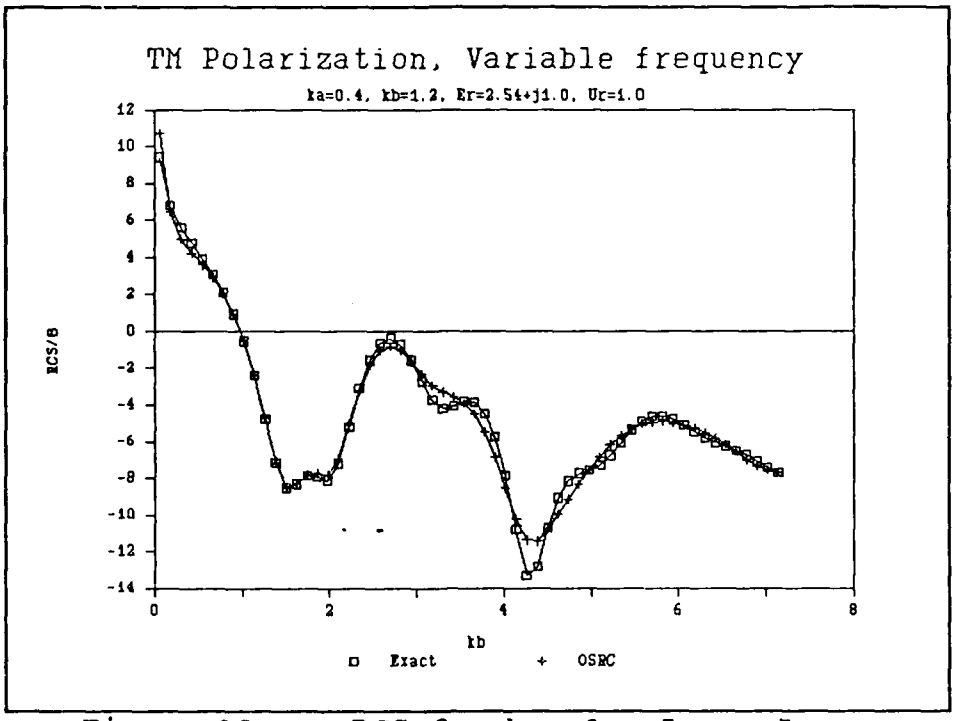

Figure 18. RCS for b = 3a, Lossy Layer

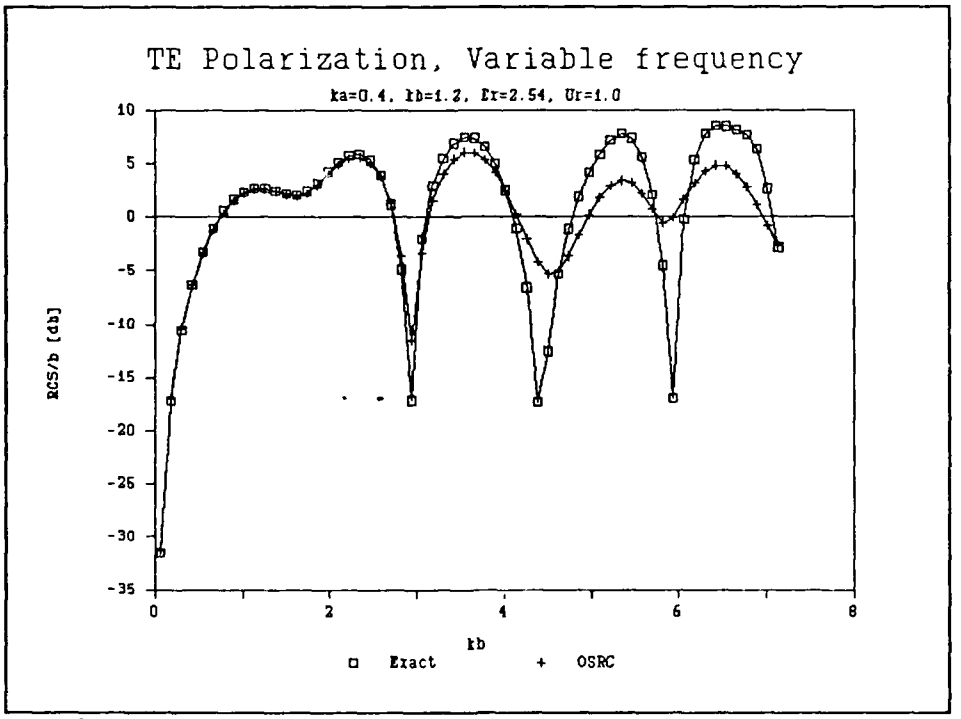

Figure 19. RCS for b = 3a, Lossless Layer

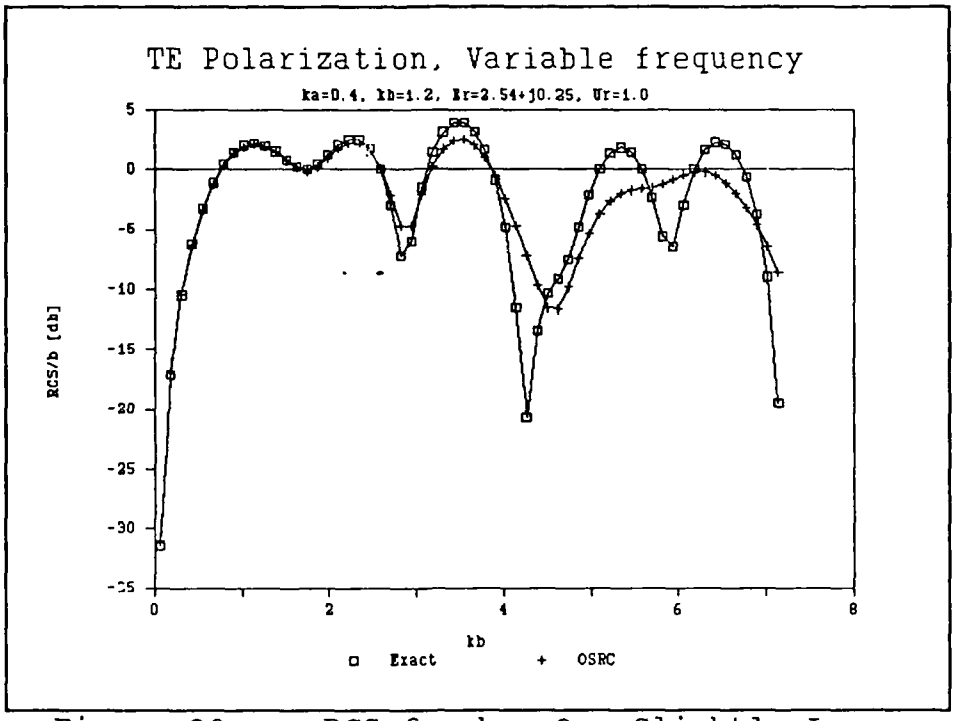

Figure 20. RCS for b = 3a, Slightly Lossy Layer

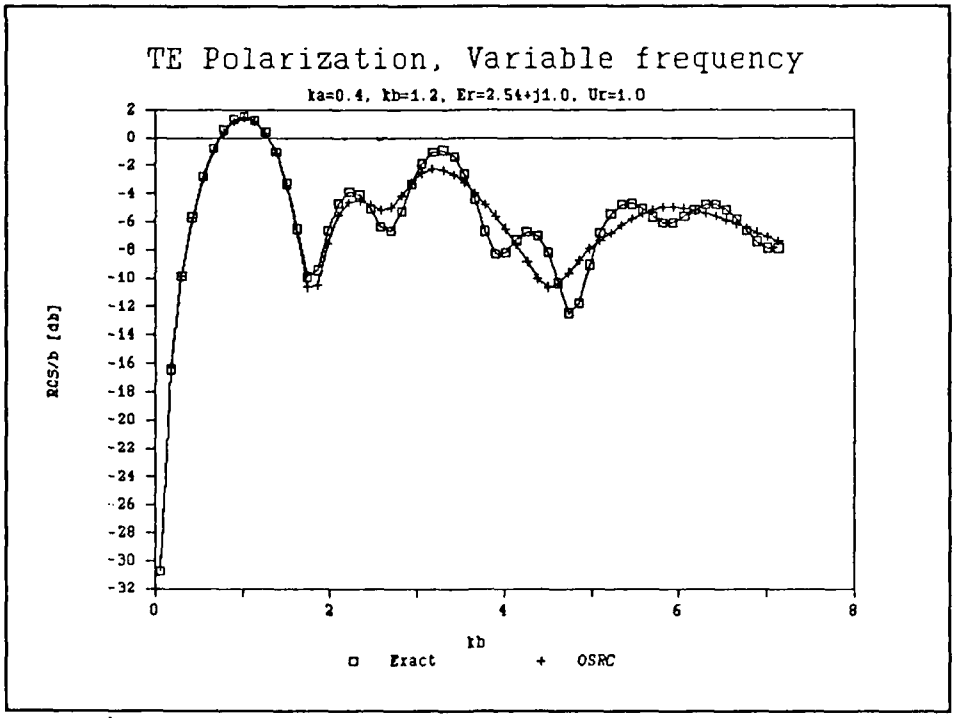

Figure 21. RCS for b = 3a, Lossy Layer

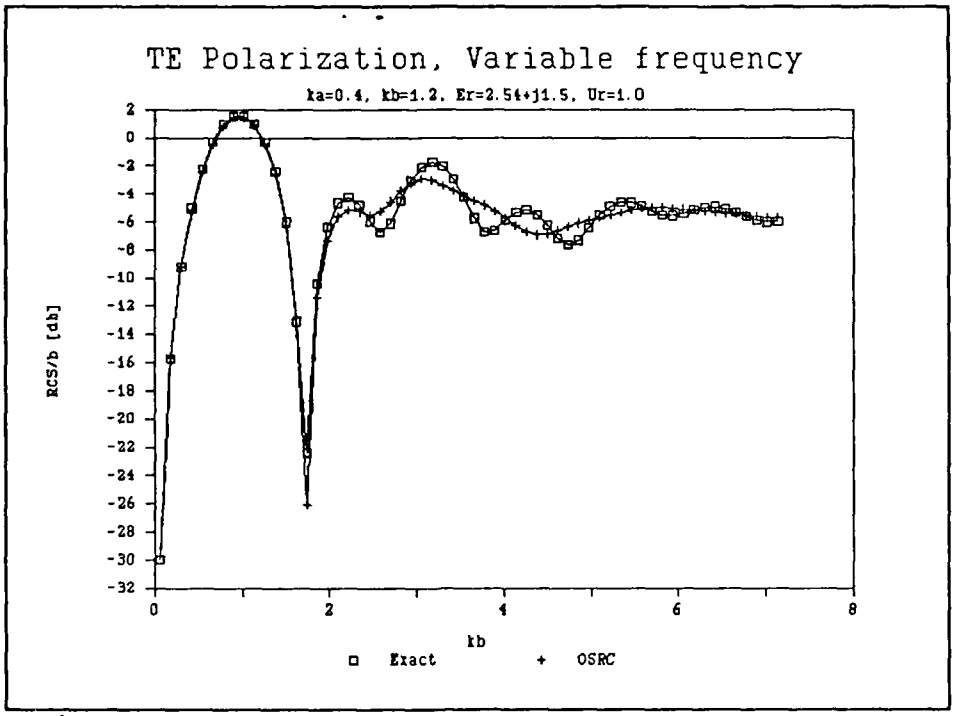

Figure 22. RCS for b = 3a, Very Lossy Layer

frequencies, the loss of the dielectric layer had to increase for the two solutions to agree over a wide range of frequencies. For TM polarization, Figure 18, the lossy case produced good agreement over all the frequencies tested. For TE polarization, the very lossy case produced good agreement over all the frequencies tested.

Figures 23 through 25 are the data for the lossless, slightly lossy and lossy cases and b = 8.5a for incident TM polarization. For all three cases, the OSRC solution agreed with the exact solution whenever kb was less than

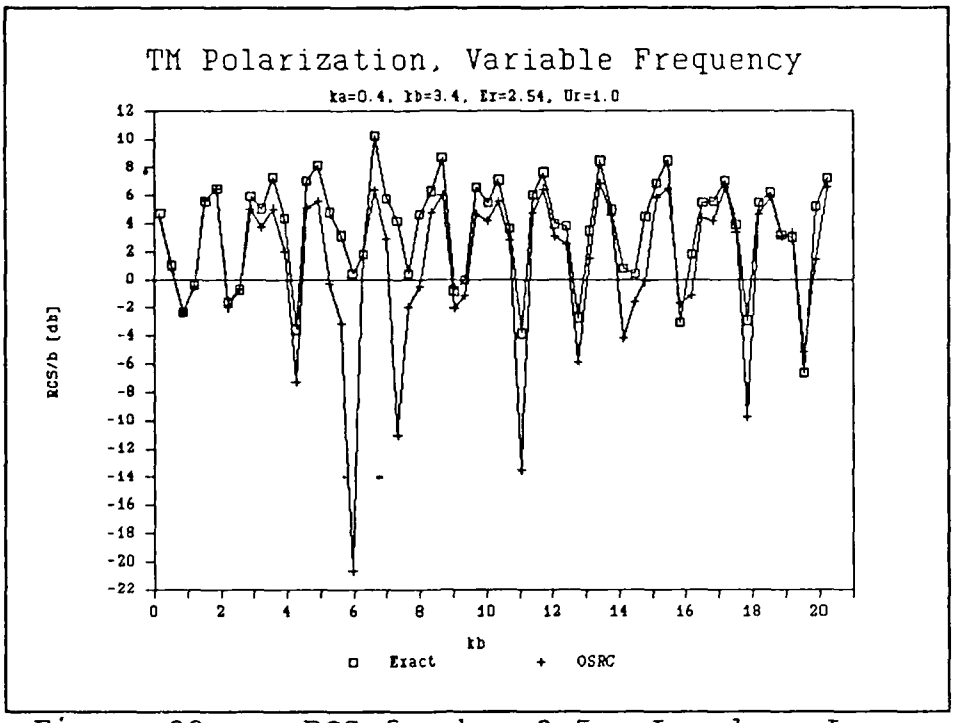

Figure 23. RCS for b = 8.5a, Lossless Layer

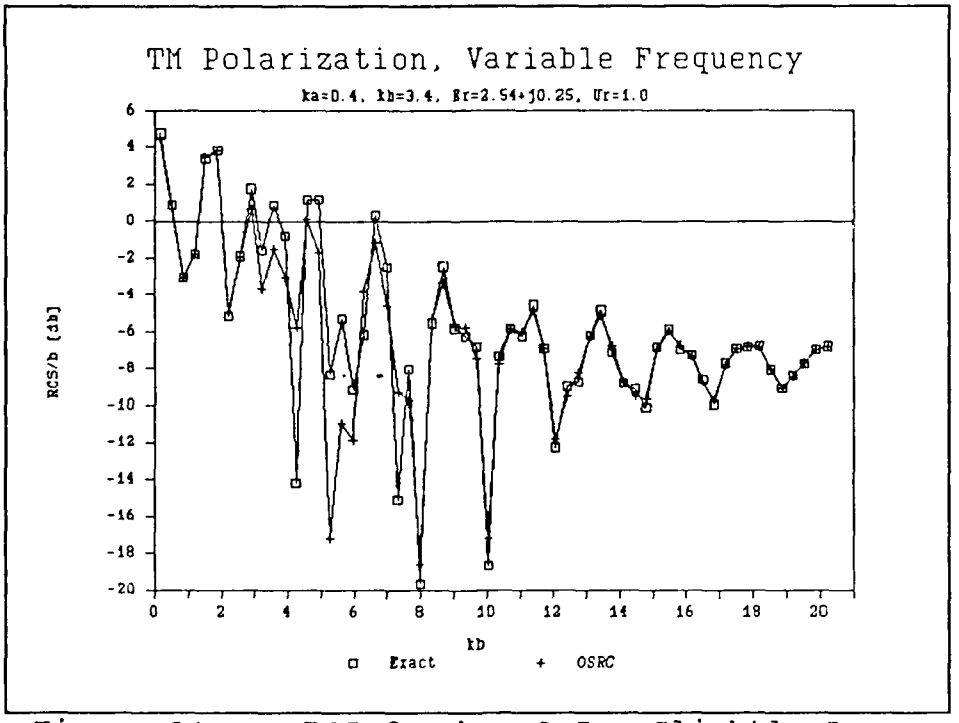

Figure 24. RCS for b = 8.5a, Slightly Lossy Layer

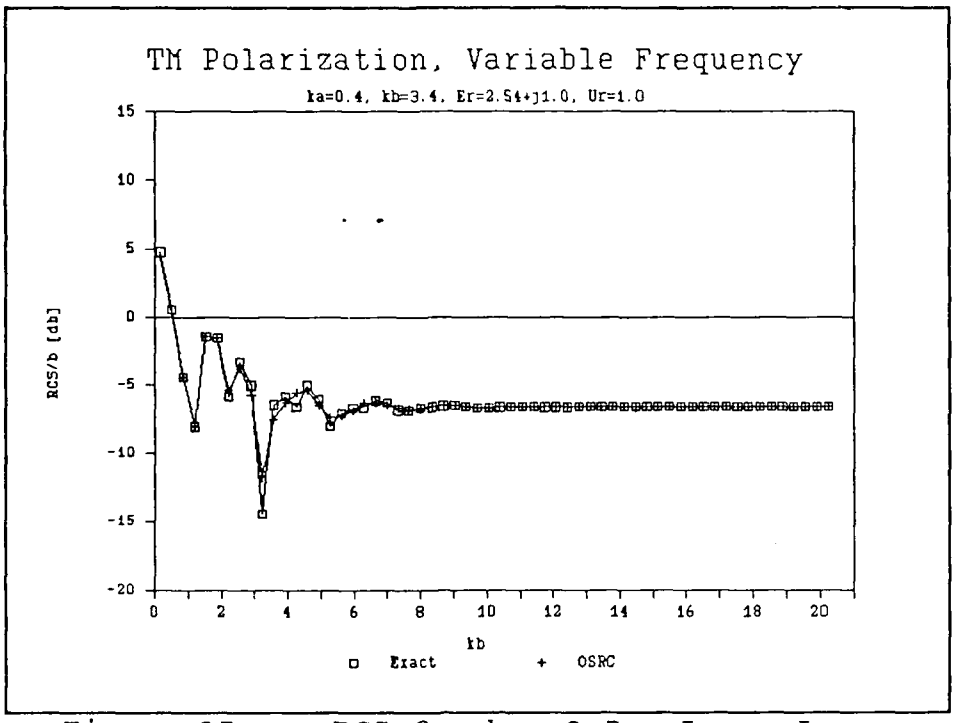

Figure 25. RCS for b = 8.5a, Lossy Layer

approximately 3.0 (thickness of the dielectric layer less than 0.4 wavelengths) or kb became "very" large (a typical high frequency approximation). For the lossless case, Figure 23, kb had to increase to 18.5 for the OSRC solution to agree with the exact solution again. For the slightly lossy case, Figure 24, kb had to increase to 8.5 for the twosolutions to agree. For the lossy case, Figure 25, the two solutions agreed for all frequencies tested.

Figures 26 through 29 are the data for all four cases and b = 8.5a for incident TE polarization. As in the TM polarization data, for kb less than 3 the OSRC solution

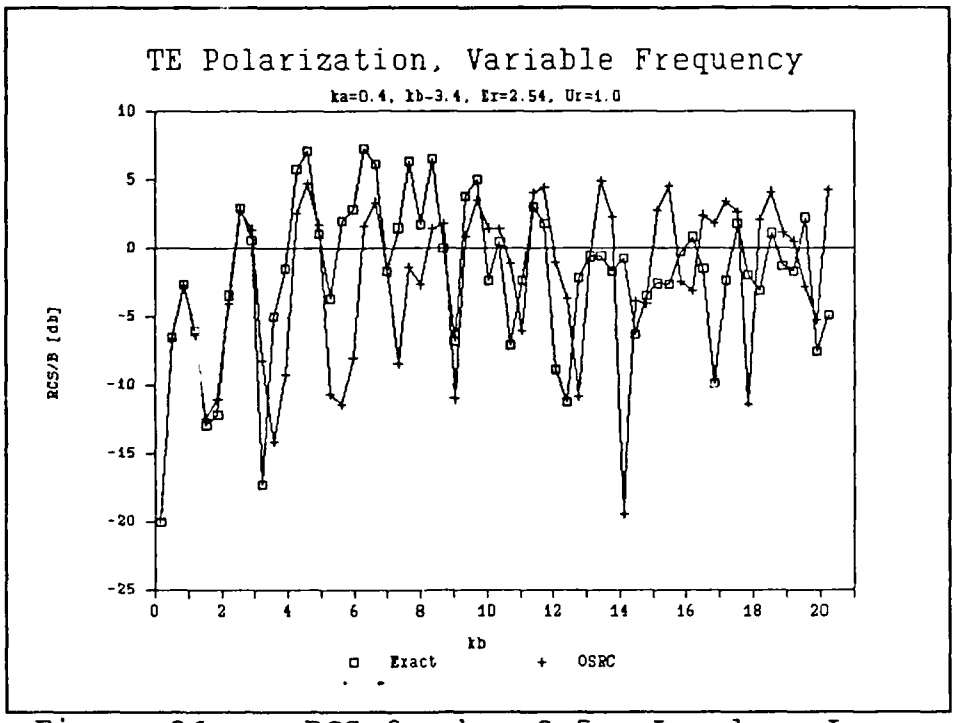

Figure 26. RCS for b = 8.5a, Lossless Layer

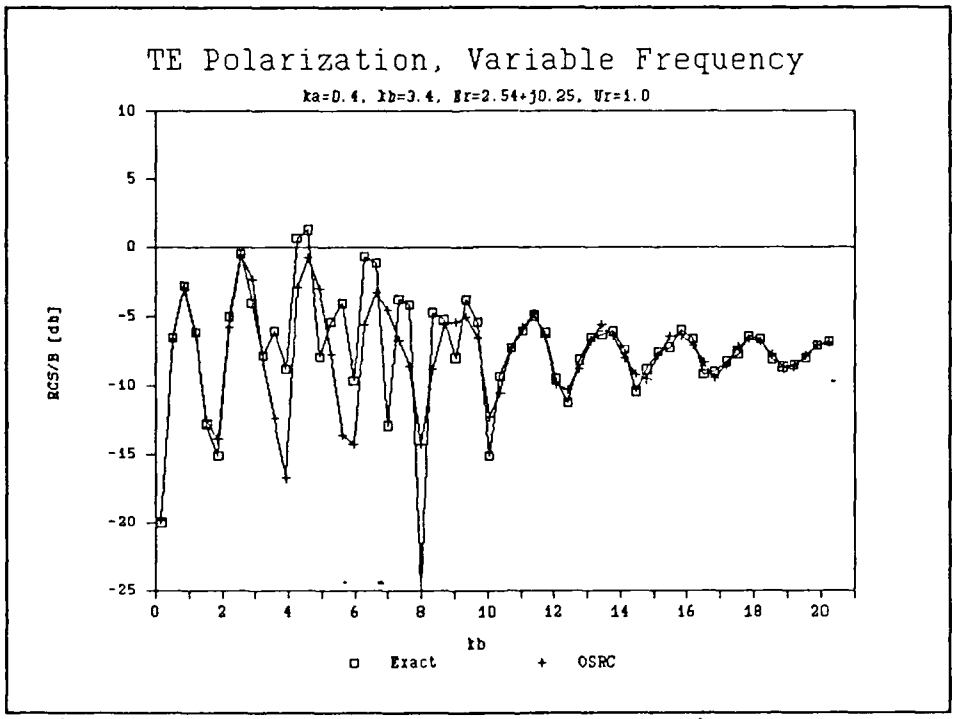

Figure 27. RCS for b = 8.5a, Slightly Lossy Layer

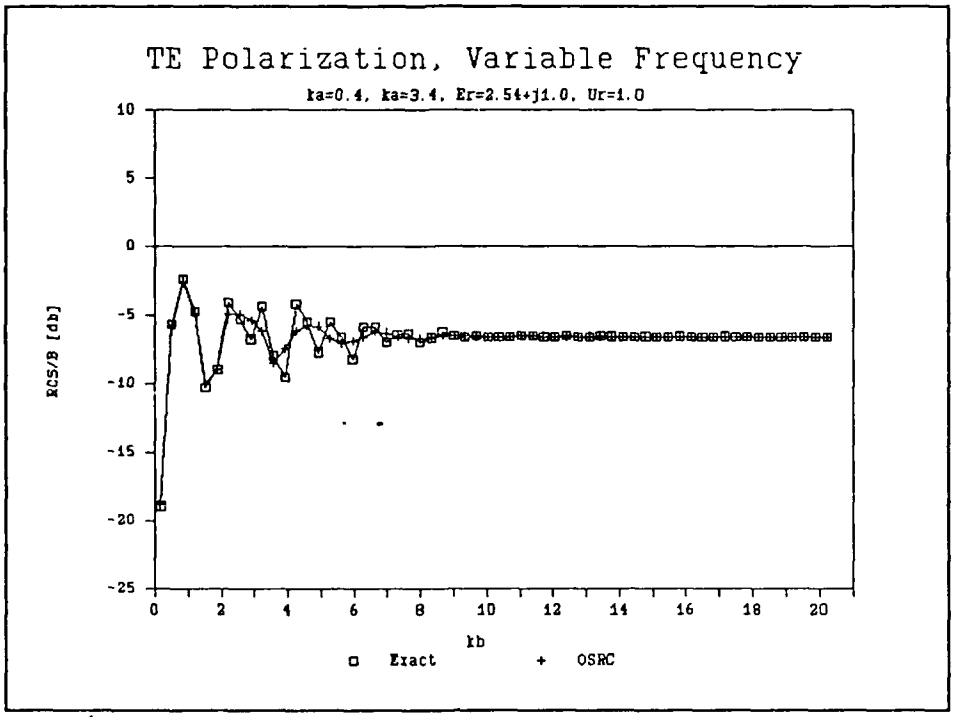

Figure 28. RCS for b = 8.5a, Lossy Layer

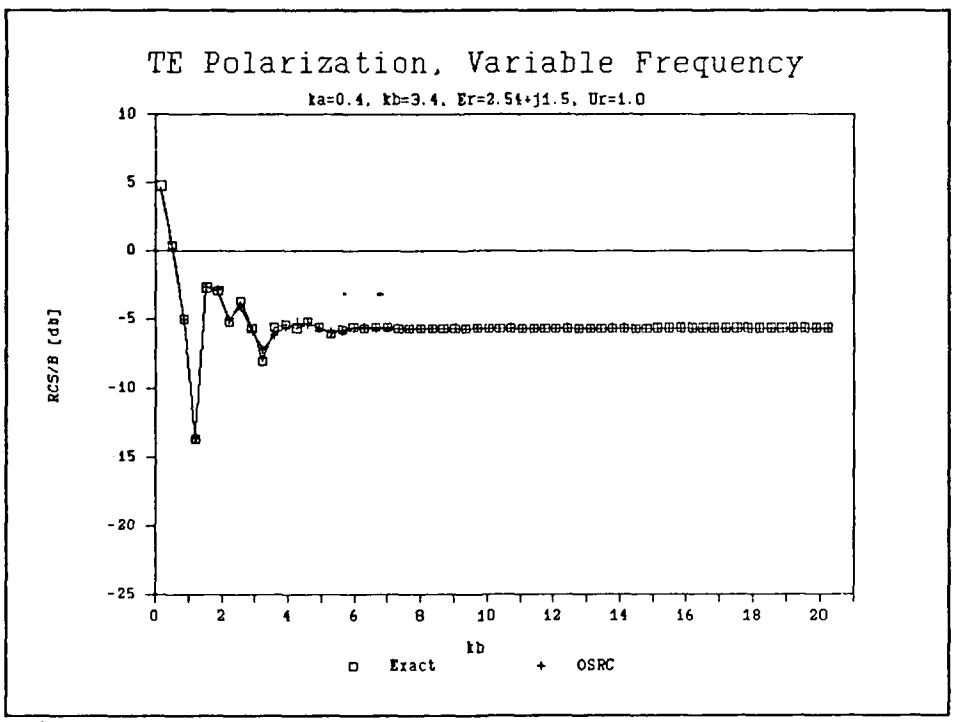

Figure 29. RCS for b = 8.5a, Very Lossy Layer

produced good results. For the lossless case, Figure 26, kb less than 3 was the only region where the OSRC solution was accurate. For the slightly lossy and lossy cases, Figures 27 and 28, the kb product had to increase to 9.0 and 6.0, respectfully, for the two solutions to agree. For the very lossy case, Figure 29, the two solutions agreed for all frequencies tested.

Bistatic Data

Figures 30 through 35 are the bistatic data for several input conditions. Figures 30 and 31 are the bistatic RCS for a "thin", lossless dielectric layer for both polarizations. The input parameters were ka = 1.57, kb = 3.0 and lossless coating. This is equivalent to a coating thickness of 0.23 wavelengths. There is excellent agreement (less than 1 db difference) for all angles. Theta equal to 180 degrees is the monostatic RCS point. Figures 32 and 33 are for a "thick", lossless dielectric layer for both polarizations. The input parameters were ka = 1.57 and kb = 6.4. This is equivalent to a coating thickness of 0.77 wavelengths. The OSRC solution had significant error for angles greater than 80 degrees for TM polarization and 100 degrees for TE polarization. The OSRC solution was accurate over a wide range of angles in the forward scattering direction for even the thick coating case. Figures 34 and

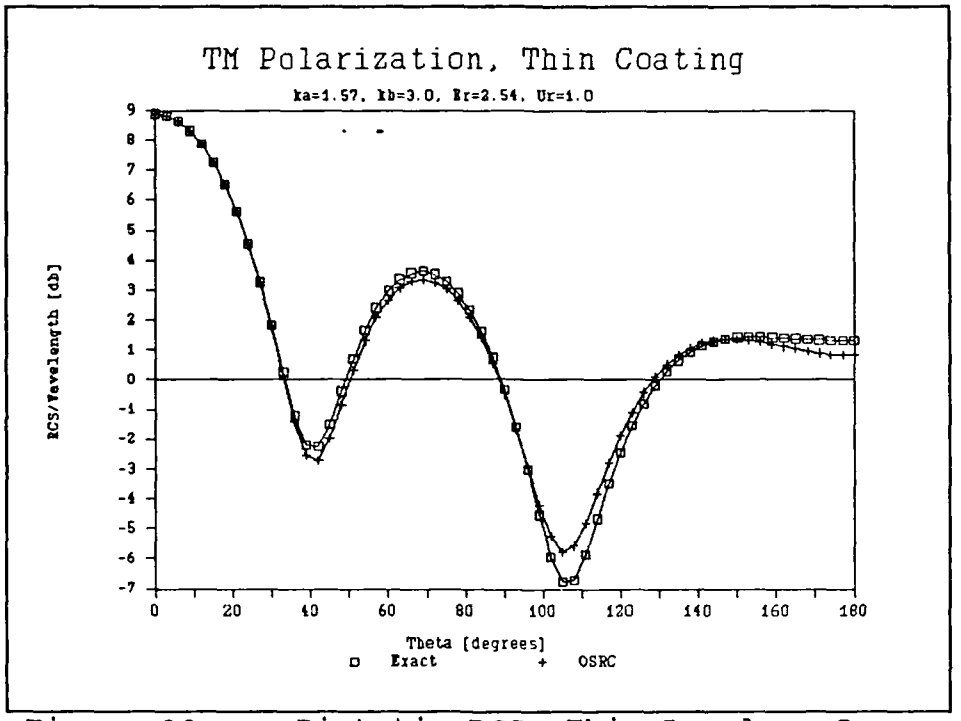

Figure 30. Bistatic RCS, Thin Lossless Layer

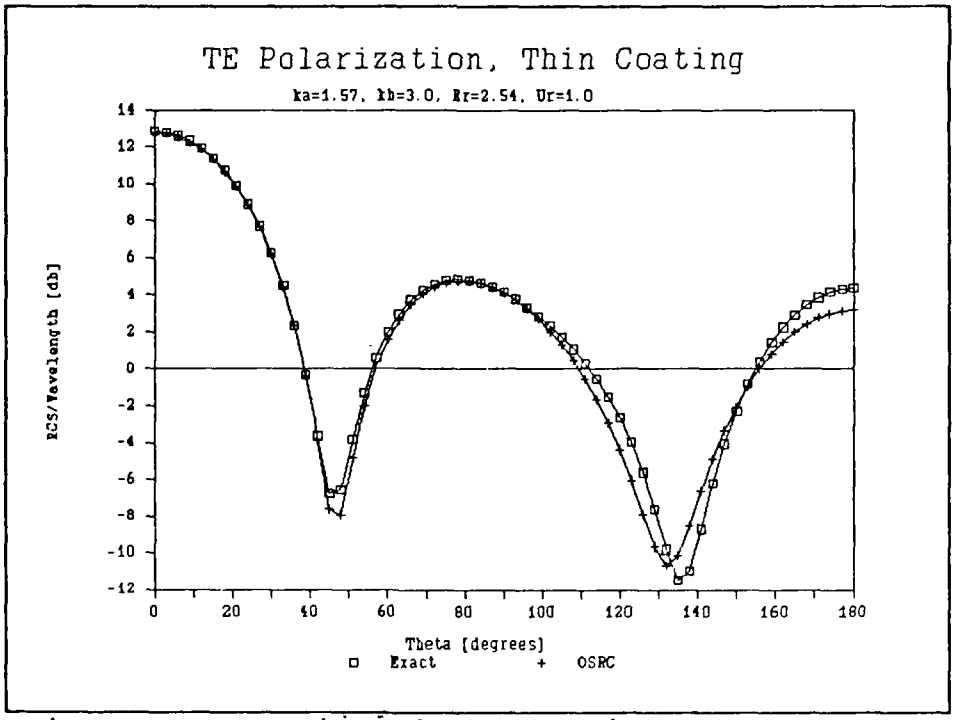

Figure 31. Bistatic RCS, Thin Lossless Layer

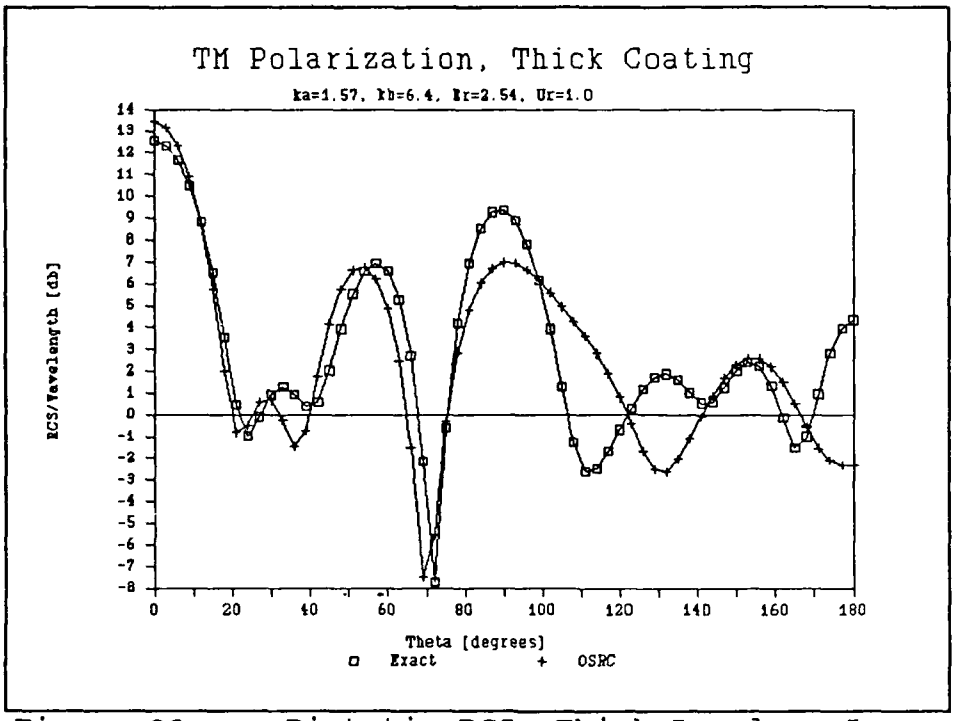

Figure 32. Bistatic RCS, Thick Lossless Layer

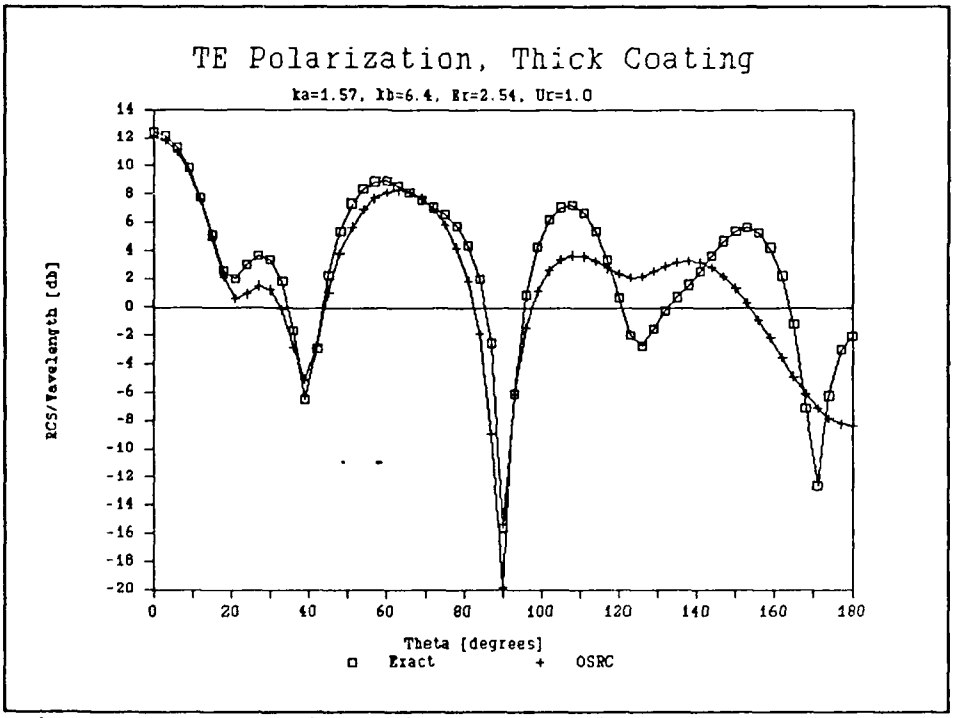

Figure 33. Bistatic RCS, Thick Lossless Layer

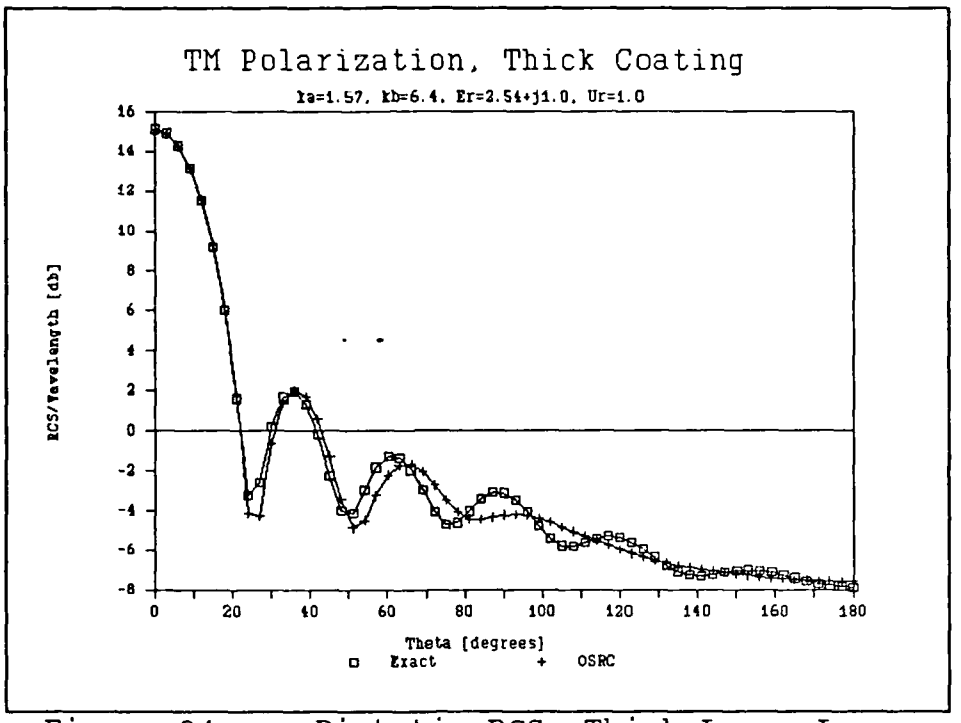

Figure 34. Bistatic RCS, Thick Lossy Layer

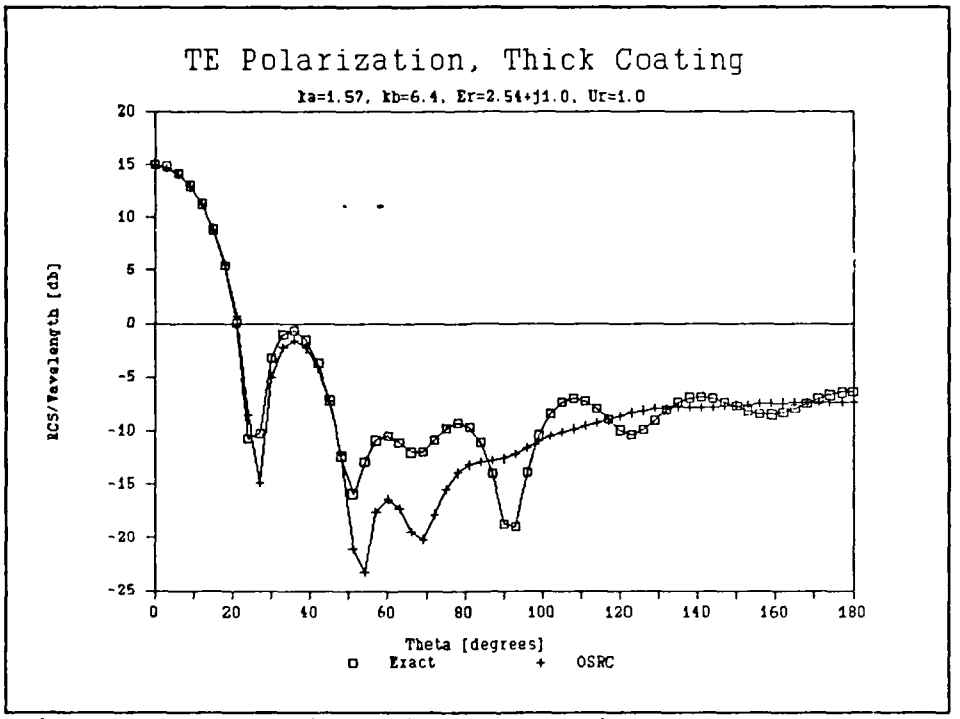

Figure 35. Bistatic RCS, Thick Lossless Layer

35 are for a "thick" , lossy layer. The input parameters are the same as for the lossless case above except for the relative permittivity. For TM polarization, the OSRC solution agreed with the exact solution for all angles. For TE polarization, the OSRC had significant error for $43° \leq \Theta \leq 130°$.

Data Analysis

As predicted by Equation 3.53, the behavior of the OSRC solution is quite complicated and depends on many different parameters. The magnitudes of kb and ka, the amount of loss and thickness of the dielectric layer all played a role in determining the overall accuracy of the OSRC solution. The mechanism which produced this error will be examined first, followed by a summary of the combinations of input parameters which produced an accurate OSRC approximation.

Only a few of the terms of the infinite series in equations 3.49 and 3.50 significantly contribute to the magnitude of the overall sum. Therefore, the error terms presented in Equation 3.53 must remain small compared to the magnitude of the coefficient for all n less than some maximum value N. In order to examine the behavior of the error in the OSRC technique as a function of n, a computer program was written to compute the error terms in Equation 3.53 for any set of input parameters. Only first two terms

of the geometric series were used. A listing of this program is included in Appendix C. Figures 36 and 37 show the results from the points kb ≈ 6.4 on Figure 4 (Figure 36), a lossless, "thick" dielectric layer example, and Figure 6 (Figure 37), a lossy, "thick" dielectric layer example. These figures indicate that the error is small for both the lossy and lossless cases for small orders, n less than 6. However, for the lossless case, the magnitude of the error grows large compared to the magnitude of the coefficient for larger orders. For example in Figure 36, the magnitude of the error exceeds the magnitude of the coefficient for n greater than 7 and is almost half the magnitude of the coefficient for n equal to 7. For the lossy case, the magnitude of the error terms also become large compared to the magnitude of the coefficient for large orders, but, the magnitude of the coefficients have decreased to the point that they do not significantly contribute to the overall sum. Figure 37 illustrates this behavior.

The behavior of the magnitude of the error terms explain why the OSRC technique is accurate for a lossy, "thick" dielectric layer and inaccurate for a lossless, "thick" dielectric layer. As the thickness increases, the number of terms which contribute to the sum, N, increases. Once N gets to approximately 7, the magnitude of the error is

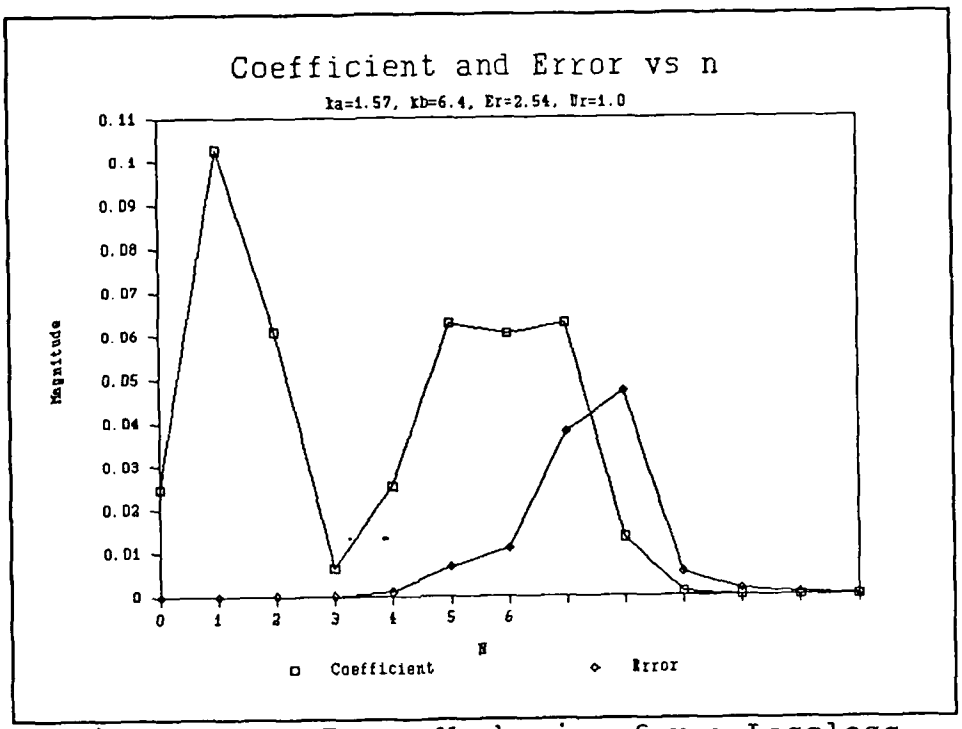

Figure 36. Error Mechanism for a Lossless Example

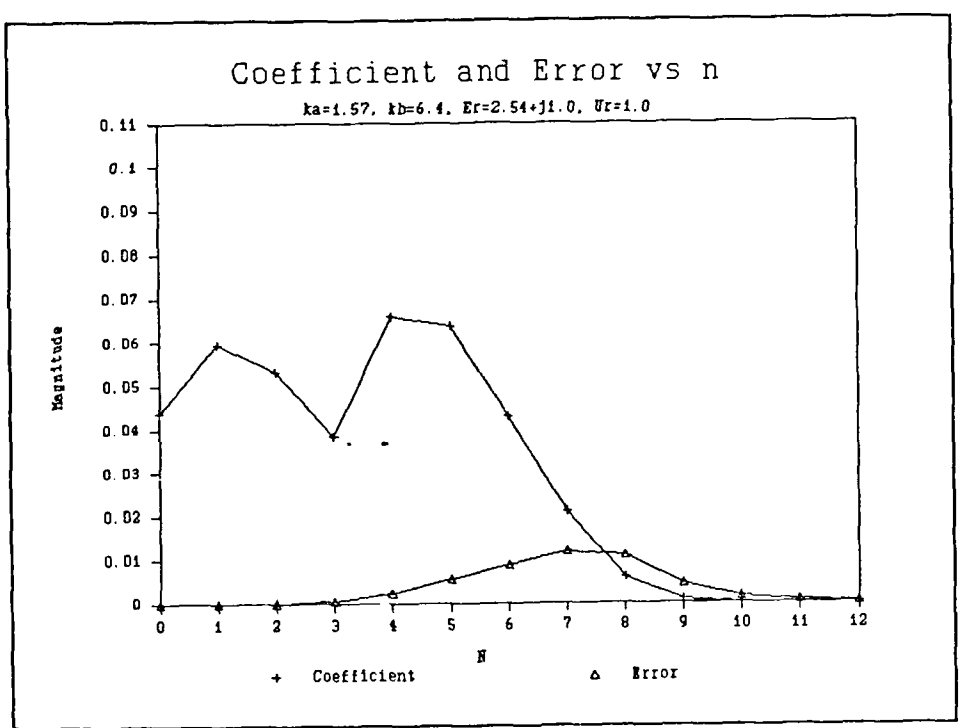

Figure 37. Error Mechanism for an Accurate Example

comparable to the magnitude of the coefficient. Loss in the dielectric layer improves this behavior because it decreases the magnitude of the higher order coefficients and the higher order error terms. Larger values of kb also improved the accuracy of the OSRC technique.

Increasing kb caused the accuracy to increase because of the e_n term in Equation 3.53. e_n is proportional to $(kb)^{-\alpha}$, where α is at least 4. If kb becomes large enough, then e_n dominates the behavior of the error and the OSRC solution is accurate. Figures 5 and 8 illustrate this behavior.

The above discussion explains the mechanism that produced the error in the OSRC technique. However, there were wide ranges of input parameters where the OSRC technique produced excellent results. Figures 38 and 39 outline the regions where the OSRC technique was found to be a good approximation for the RCS of a dielectric coated circular cylinder for both TM and TE polarizations. The minimum value for kb is ka (a = b) for any given geometry and frequency. Using the data presented above and extra data generated from the variable thickness programs, the ranges of input parameters which produced less than 2 db of error were plotted. These regions were divided along lines of constant ka for varying kb and loss. Any combination of geometry, frequency and loss which occurs above its line of constant ka on Figure 36 or 37 should produce an OSRC

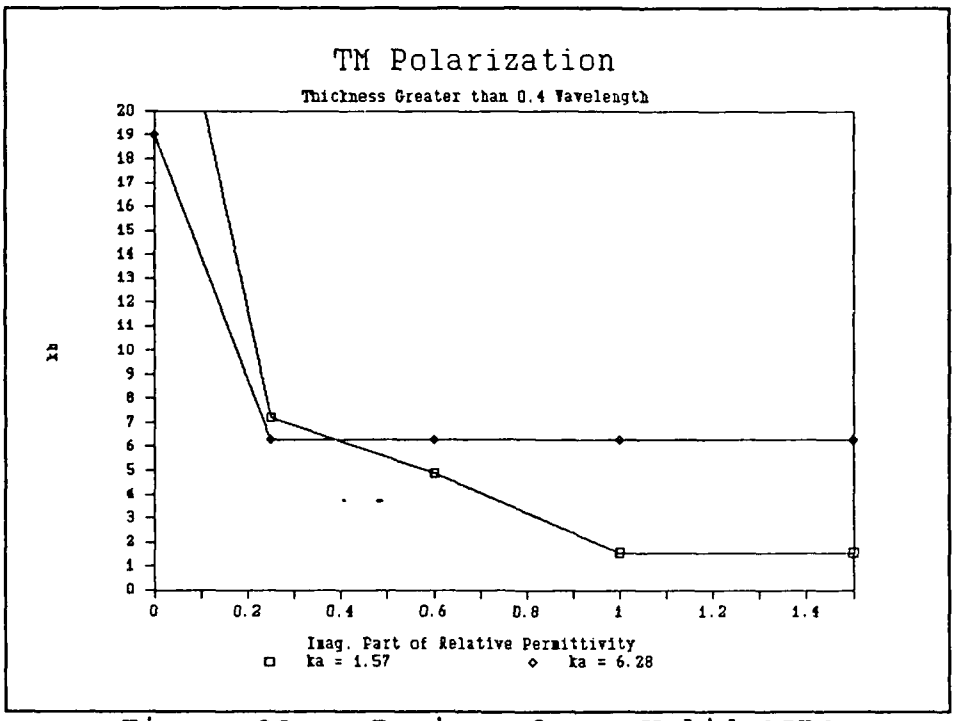

Figure 38. Regions for a Valid OSRC Approximation

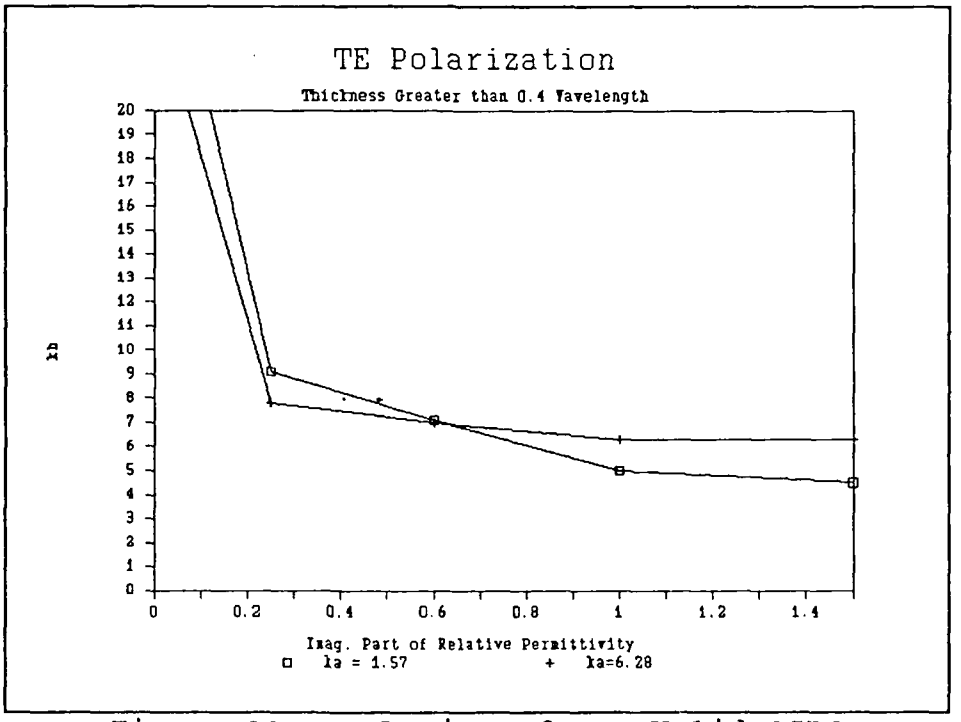

Figure 39. Regions for a Valid OSRC Approximation

approximation which has less than 2 db of error. Based on the results presented in Figures 36 and 37, several generalizations about the accuracy of the OSRC technique are possible.

The data presented above indicates that in order for the OSRC technique to agree with the eigenfunction solution one of several possible conditions must be true. The first condition for a valid OSRC solution was a "thin" layer. If the dielectric layer was less than about 0.4 wavelengths for incident TM polarization, then the OSRC solution was valid. If ka was approximately equal to 1.57 for incident TE polarization and the the thickness of the dielectric layer was less than 0.4 wavelengths, then the OSRC approximation was good. Another condition for a valid OSRC solution wassignificant loss in the dielectric layer. The OSRC solution produced a good approximation to the RCS whenever the imaginary part of the relative permittivity was increased beyond a maximum value. This maximum value was 1.0 for incident TM polarization or 1.5 for incident TE polarization. A third condition was for a very large kb product. However, there was no simple relationship which predicts how large kb must be in order for the OSRC technique to have less than 2 db of error.

Summary

Comparisons between the OSRC solution and the eigenfunction solution were presented. The OSRC solution was found to agree with the eigenfunction solution for wide ranges of input parameters. In general these parameters were the thickness of the dielectric layer less than 0.4 wavelengths, the magnitude of the imaginary part of the relative permittivity greater than 1.0 for incident TM polarization or 1.5 for incident TE polarization, or the kb product "very" large. Data was presented which outlined which combinations of geometry, dielectric material loss and frequency will produce a valid OSRC approximation for the RCS of a dielectric coated cylinder.

V. Conclusions and Recommendations

The OSRC technique can be used to predict the RCS of dielectric coated cylinders if certain conditions are true. Figures 38 and 39 summarize the regions of validity of the OSRC technique for this problem. The behavior of the OSRC solution was correct for even surprisingly small values of kb. However, the behavior was incorrect for large orders. This combination of behaviors made it very difficult to define a simple region of validity based on frequency alone. Thus, Figures 38 and 39 illustrate which combinations of loss, frequency and thickness of the dielectric layer produced accurate results. The data and analysis presented in Chapter 4 are consistent with a physical understanding of the behavior of the field in the dielectric material. Before summarizing the results, a brief discussion of these physical mechanisms will be presented.

The OSRC technique produced accurate results for incident TM polarization and a thin layer because the specular return from the surface of the cylinder dominates the RCS for this set of conditions. The specular return consists of the lower order modes (small indices) of the infinite series. Since the OSRC technique has the correct behavior for the lower order modes, there was minimal error

in the OSRC solution for this set of conditions.

Incident TE polarization is much more likely to excite traveling waves or creeping waves on the surface of the conducting cylinder since there is a component of the electric field along the surface in the direction of propagation (Knott and others, 1985:166). These surface waves are higher order modes (large indices) of the infinite series and, as explained above, the OSRC technique does not behave well for higher order modes. This explains why in Figures 13 and 14 the error was large for thin layers; creeping waves are contributing significantly to the RCS and the OSRC technique does not approximate these higher order modes well. Another mechanism which produces significant higher order modes in the dielectric layer is multiple reflections between the dielectric layer and the conducting surface.

Using geometrical optics terminology, an incoming ray is both transmitted and reflected at the dielectric/free space boundary. The transmitted ray is then reflected at the conductor surface and sent back to the dielectric boundary where it is both transmitted into free space and reflected back to the conductor surface. The reflected ray propagates back to the conductor surface where it is reflected again and sent back to the dielectric boundary. This multiple reflection process continues with the magnitude of the

reflected ray decreasing with each reflection at the dielectric boundary. As the thickness of a lossless layer increases, the contribution to the RCS from these multiple reflections increases. One reason this occurs is simply because the dielectric surface intercepts a larger portion of the incident plane wave. These multiple reflections are higher order modes of the infinite series and the error in the OSRC approximation is significant for these modes. If there is loss in the dielectric layer, these multiple reflections are attenuated with each pass through the layer, thus reducing their contribution to the RCS. This physical argument explains why the error in the OSRC approximation gets large as the thickness of the dielectric layer increases. These multiple reflections are higher order modes of the infinite series and, as explained many times above, the OSRC approximation falls apart when the higher order modes have a significant contribution to the RCS. Loss in the dielectric layer reduces the contribution of these higher order modes more than the lower order modes and thus reduces the error in the OSRC approximation. This behavior is independent of polarization, and examination of the data in Chapter 4 is consistent with this explanation. With the above understanding of the physical mechanisms within the dielectric layer and the results of the data analysis, it is possible to make some generalizations about

the behavior of the OSRC approximation.

One possible generalization was if the imaginary part of the relative permittivity was greater the 1.0 for incident TM polarization or 1.5 for incident TE polarization, then the OSRC technique produced a good approximation for the RCS, even when the size of the cylinder was in the resonance region. Since TE polarization tends to excite the higher order modes in the dielectric layer more than TM polarization, TE polarization should require more loss to achieve the same degree of accuracy. This is consistent with the observed behavior. Many of the materials used for absorbing coatings meet these requirements for the imaginary part of the relative permittivity over a wide range of frequencies (Joseph, 1986:53-57 and Eccosorb, 1980:5-20).

Another possible generalization was if the thickness of the dielectric layer was less than 0.4 wavelengths then the OSRC approximation was accurate for TM polarization. This result is very similar to the range of accuracy found by Wang for the geometrical optics approximation (Wang, 1985: 962). This similarity may be due to the fact that both techniques are essentially high frequency approximations.

The problems of numerical instabilities near interior resonance regions that occurs for MM solutions (Wu and Tsai, 1977:520-523) were not observed. Whenever the input parameters were such that the error was less than 2 db, the

OSRC solution was accurate even when there was a great deal of cancellation of the fields. However, these deep null regions were the last areas to converge to the exact solution as the parameters changed. The OSRC technique can be a valuable tool for cases where absorbing material has been applied to a conducting surface.

The OSRC solution did not converge any faster than the eigenfunction solution. The number of terms in the infinite series which had significant contributions to total sum was approximately the same for both solutions. Based on this fact, the OSRC approximation showed no improvement in numerical efficiency over the exact solution. However, the OSRC technique is amenable to non-circular geometries while the eigenfunction solution is obviously not.

Based on the results presented above, there is considerable motivation for continuing work with the OSRC approximation technique. The real advantage to using this technique should be for non-circular geometries where an exact solution is not known. Therefore, the first recommendation for future work is to apply the OSRC technique to an elliptical cylinder coated with an elliptical dielectric layer. A numerical solution of the interior problem using an OSRC boundary operator in lieu of a radiation condition can be used to find values for the fields on the surface of the dielectric material. Once

these are known, a quadrature technique can be used to find a numerical approximation to the RCS based on the OSRC integral equations from Chapter 3.

Another recommendation for future work is to extend the present work using OSRC to three dimensions. A spheroidal shape would be an excellent starting point for three dimensional problems because the radius of curvature is continuous over the entire surface. A closed form approximation for the RCS may be achievable using the OSRC technique.

A less ambitious project would be to use the programs developed in this project to investigate how well the OSRC technique performs for magnetic coatings. Since magnetic coatings are generally used to reduce traveing or creeping waves (Knott and others, 1985:253), the OSRC approximation may perform better for this class of coatings.

Appendix A: Derivation of the OSRC Operator

In this Appendix the motivation for using an OSRC boundary operator is explained and the second order operator for a two dimensional field is derived.

Since the scattered field must satisfy the Sommerfield radiation condition, it can be expressed as:

$$\Phi^s = \frac{e^{jkr}}{r^{1/2}} \left[A_0 + \frac{A_1}{r} + \frac{A_2}{r^2} + \ldots \right] \quad \text{(A.1)}$$

where,

k = wave number

r = cylindrical coordinate radial distance

Equation A.1 is valid for two dimensional fields; for three dimensional fields, the square root of r is replaced by r. Colton and Kress have shown that, as a consequence of the radiation condition, this series converges absolutely and uniformly and can be differentiated term by term with respect to any of the coordinate system variables to produce a series which converges absolutely and uniformly (Colton and Kress, 1983:72-74). The n^{th} order OSRC differential operator uses this fact to find an approximation for the normal derivative of the scattered field by taking n derivatives of Equation A.1 mutliplied by $e^{-jkr}\, r^{n-1/2}$. The error in this approximation is proportional to $r^{-2n-1/2}$.

This approximation for the normal derivative is used in the integrand of an integral equation representation for the scattered field to find an approximation for the scattered field (Kriegsmann and others, 1987:155). The details of the derivation of the second order OSRC operator follow.

For n = 2, Equation A.1 is multiplied by $e^{-jkr}\, r^{3/2}$:

$$e^{-jkr}\, r^{3/2}\, \Phi^s = \left[A_0 r + A_1 + \frac{A_2}{r} + \frac{A_3}{r^2} + \ldots \right] \qquad (A.2)$$

Taking two derivatives with respect to r gives:

$$\frac{\delta^2}{\delta r^2} \left[e^{-jkr}\, r^{3/2}\, \Phi^s \right] = O(r)^{-3} \qquad (A.3)$$

where $O(r)^{-n}$ implies the series behaves as r^{-n} as r goes to positive infinity. Expanding the left hand side of Equation A.3:

$$r^{3/2}\, e^{-jkr} \left\{ \frac{\delta^2 \Phi^s}{\delta r^2} + \frac{\delta \Phi^s}{\delta r} \left(3r^{-1} - 2jk \right) + \Phi^s \left(\frac{3}{4} r^{-2} - 3jkr^{-1} - k^2 \right) \right\} = O(r^{-3}) \qquad (A.4)$$

Since Φ^s must satisfy the homogenous Helmholtz equation, an expression for the second partial derivative of the scattered field with respect to r can be found by expanding the Laplacian operator in cylindrical coordinates and rearranging terms.

$$\frac{\delta^2 \Phi^s}{\delta r^2} = - r^{-1} \frac{\delta \Phi^s}{\delta r} - r^{-2} \frac{\delta^2 \Phi^s}{\delta^2} - k^2 \Phi^s \quad (A.5)$$

Substituting Equation A.5 into Equation A.4, dividing by $r^{3/2} e^{-jkr}$ and simplifying the resulting expression produces the second order OSRC operator, B_2.

$$B_2 \{ \Phi^s \} = O(r^{-4.5}) \quad (A.6)$$

where,

$$B_2 = \frac{\delta}{\delta r} + \frac{1}{2r} - jk - \left(\frac{\delta^2}{\delta^2} + \frac{1}{4} \right) [2r(1 - jkr)]^{-1}$$

Notice that setting $B_2 \{ \Phi_s \} = 0$ will produce an error term that is proportional to $r^{-4.5}$.

Appendix B. Bessel Function Subroutines

The algorithms used to compute the Bessel's functions were adapted from the method described by Kelly (Kelly, 1967:239-241). It is assumed that only integer orders are required and the maximum order (N) is known a priori. The algorithms are valid for either real or complex argument and a different set of programs was written for the two cases. The programs were written in Fortran 77 and run on an IBM PC machine. A listing of the subroutines is included. The method used to find the Bessel functions of the first kind ($J_n(z)$) will be described first, followed by a description of the method used to find the Bessel functions of the second kind ($Y_n(z)$).

The Bessel functions of the first kind are found using backward recurrsion and a modified form of Gegenbauer's formula to find the normalization constant. The recursion relation is initialized by:

$$\hat{J}_{N+12}(z) = 0 \qquad \text{and} \qquad \hat{J}_{N+11}(z) = 10^{-37}$$

Then the initial values for $J_n(z)$ are computed from:

$$\hat{J}_{n-1}(z) = (2n/z)\hat{J}_n(z) - \hat{J}_{n+1}(z) \qquad (B.1)$$

for $1 \leq n \leq N+10$. The upper limit of N+10 was chosen to ensure the accuracy of the highest order Bessel function required for use by the calling program. These initial values are used in a modified form of Gegenbauer's formula to find the normalization constant.

Kelly gives Gegenbauer's formula as:

$$\sum_{n=0}^{\infty} \frac{(2n+\alpha)\ \Gamma(n+\alpha)}{n!}\ (2/z)^{\alpha}\ J_{2n+\alpha}(z) = 1 \qquad (B.2)$$

where $\Gamma(x)$ is the Gamma function. For n a positive integer and $\alpha = 1$, This equation reduces to:

$$(2/z) \sum_{n=0}^{n=\infty} (2n+1)\ J_{2n+1}(z) = 1 \qquad (B.3)$$

Since the $\hat{J}_n(z)$ satify the reccurrence relation, they must be equal to a constant times the Bessel function.

$$J_n(z) = K\ \hat{J}_n(z) \qquad (B.4)$$

Substituting Equation B.4 into Equation B.3, we can solve for the constant K.

$$K = \left[(2/z) \sum_{n=0}^{n=\infty} (2n+1)\ \hat{J}_{2n+1}(z) \right]^{-1} \qquad (B.5)$$

Since only a finite number of Bessel functions can be computed, the upper limit of the summation is M=(N+10-1)/2 and Equation B.5 is an approximation for K.

Once K is found, each $\hat{J}_n(z)$ is multiplied by K for an approximation to $J_n(z)$ and $J_0(z)$ is found from Equation B.1.

Once the $J_n(z)$ are known, the $Y_n(z)$ are found by first computing $Y_0(z)$ and then using the Wronskian relation to find the rest of the $Y_n(z)$. $Y_0(z)$ is computed using the following formula (Abromawitz and Stegun, 1972:360):

$$Y_0(z) = 2/\pi[\{\ln(z/2)+\delta\}J_0(z) + \frac{(z/2)^2}{(1!)^2} - (1+1/2)\frac{(z/2)^2}{(2!)^2} +$$

$$(1+1/2+1/3)\frac{(z/2)^2}{(3!)^2} - \ldots\ldots\ ] \qquad (B.6)$$

where δ = Eulers constant. Forward recurrsion through the Wronskian equation is used to compute the rest of the $Y_n(z)$'s.

$$Y_{n+1}(z) = \{\ J_{n+1}(z)Y_n(z) - [2/(\pi z)]\ \}/\ J_n(z) \qquad (B.7)$$

The above equations were implemented in the subroutines JNZ, YNZ and Y0F for complex argument and JNX, YNX and Y0FX for real argument using double precision arithmetic. The values for the Bessel's functions produced by these subroutines were checked against the National Bureau of Standards tables (Abromawitz and Stegun, 1972:370-383) for arguments of 0.5, 2.0 and 10.0 and orders 0 through 40. The worst case error found was 10^{-5} when the requested order was at least larger than the magnitude of the requested argument plus three. A listing of the programs follows.

```
      Subroutine JNZ(Z,J,J0,K)
 Computes integer order Bessel functions (first kind) for
c       complex argument.
c    Z   =  argument of the Bessel Function
c    J   =  Complex valued array of integer order Bessel
c    functions K   =  Integer comtaining value of the highest
c     order Bessel function to be computed
c
      Complex*16 Z,J(101),SUM,F,J0
      Integer K,LK
```

```
      LK=K+10
      IF(float(LK)/2.0.eq.INT(LK/2.0)) LK=LK+1
      J(LK+2)=(0.0,0.0)
      J(LK+1)=(1.0E-37,0.0)
      do 10 I = LK,1,-1
         J(I)=2.0*Float(I+1)/Z*J(I+1)-J(I+2)
10    continue
      sum=J(1)+3.0*J(3)
      do 20 I = 2,(LK-1)/2
         sum=sum+J(2.0*I+1)*(1.0+2.0*Float(I))
20    continue
      sum=sum*(2.0/Z)
      do 30 I = 1,K
         J(I)=J(I)/sum
30    continue
      J0=(2.0/Z)*J(1)-J(2)
      return
      end
c
c
c
      Subroutine YNZ(Z,J,J0,Y,Y0,N)
      Complex*16 Z,J(101),J0,Y(101),Y0,Y0F
      Integer N
      PI=3.14159265
      Y0=Y0F(Z,J0,N)
      Y(1)=(Y0*J(1)-2.0/PI/Z)/J0
      Do 10 I=2,N
         Y(I)=(Y(I-1)*J(I)-2.0/PI/Z)/J(I-1)
10    Continue
      return
      end
c
c
      Complex*16 Function Y0F(Z,J0,N)
c   Computes zeroth order Bessel function of the second
c   kind. Required input is the complex valued argument,
c   zeroth order Bessel's function of the first kind
c   evaluated at that argument and the highest integer to
c   sum to (converges at 1/factorial squared)
c
      Complex*16 Z,J0,sum,numer
      Double precision K,PI,Eulers,denom,factor
      Integer N
      PI=3.14159265
      Eulers=0.57721566490153
c
c  initialize constants used in the summing loop
c
      sum=(0.0,0.0)
```

```
      numer=Z**2.0/4.0
      denom=1.0
      factor=0.0
      do 10 I=1,N
         K=float(I)
         Factor=Factor+1.0/K
         denom=denom*K
         sum=sum+(-1.0)**(I-1)*Factor*numer**I/denom**2.0
10    continue
      Y0F=2.0/PI*((cdlog(Z/2.0)+Eulers)*J0+sum)
      return
      end
c
c
c
      Subroutine JNX(X,J,J0,K)
c       Computes integer order Bessel functions (first kind)
c   for real argument.
c
c   X   =  argument of the Bessel Function
c   J   =  Complex valued array of integer order Bessel
c   functions K   =  Integer containing value of the highest
c   order Bessel function to be computed.
c
c
      Double Precision X,J(101),SUM,J0
      Integer K,LK
      LK=K+10
      IF(float(LK)/2.0.eq.INT(LK/2.0)) LK=LK+1
      J(LK+2)=(0.0,0.0)
      J(LK+1)=(1.0E-37,0.0)
      do 10 I = LK,1,-1
         J(I)=2.0*Float(I+1)/X*J(I+1)-J(I+2)
10    continue
      sum=J(1)+3.0*J(3)
       do 20 I = 2,(LK-1)/2
         sum=sum+J(2.0*I+1)*(1.0+2.0*Float(I))
20    continue
      sum=sum*(2.0/X)
      do 30 I = 1,LK
         J(I)=J(I)/sum
30    continue
      J0=(2.0/X)*J(1)-J(2)
      return
      end
c
c
      Double Precision Function Y0FX(X,J0,N)
c   Computes zeroth order Bessel function of the second
c   kind.
```

```
c   Required input is the real valued argument, zeroth order
c   Bessel's function of the first kind evaluated at that
c   argument and the highest integer to sum to (converges at
c   1/factorial squared)
c
      Double precision  K,PI,Eulers,denom,numer
      Double Precision  factor,X,J0,sum
      Integer N
      PI=3.14159265
      Eulers=0.57721566490153
c
c  initialize constants used in the summing loop
c
      sum=(0.0,0.0)
      numer=X**2.0/4.0
      denom=1.0
      factor=0.0
      do 10 I=1,N
         K=float(I)
         Factor=Factor+1.0/K
         denom=denom*K
         sum=sum+(-1.0)**(I-1)*Factor*numer**K/denom**2.0
10    continue
      Y0FX=2.0/PI*((dlog(X/2.0)+Eulers)*J0+sum)
      return
      end
```

Appendix C. Listing of Computer Programs

All of the programs were writen in FORTRAN 77 and implemented on an IBM PC computer. Since the code for most of the programs is very simimlar, only four programs are listed here. Three of the programs are the programs used to calculate the eigenfunction solution and the two OSRC solutions for the increasing thickness data. The fourth program is the program used to find the error terms in the OSRC technique as a function of the order. The only difference between the listed code and the other programs is the variable which was changed after each loop.

The first program is the eigenfunction solution for the RCS of a dielectric coated cylinder derived in Chapter 3.

```
c234567890
      Program DICYLV1
      Complex*16 JNK2B(101),J0K2B,JNK2A(101),J0K2A
      Complex*16 YNK2B(101),Y0K2B,YNK2A(101),Y0K2A
      Complex*16 JNPK2B,YNPK2B,JNPK2A,YNPK2A,Index,K2,ANND
      Complex*16 K2A,K2B,CDSUM,J,DN(2),AN,ANN,Er,Ur,Pr
      Double Precision PI,JNPM,JN(101),J0,theta
     .Double Precision YNK1B(101),Y0K1B,K1B,YNPK1B
      Double Precision Cond,K1,A,B,Eo,c,DeltaB,X
      Integer N,L,M,POL
      open(8,file='outexv1.prn')
      open(9,file='inv2.dat')
c
c  Initialize constants
c
      PI=3.14159265
      c=3.0E+08
      Eo=8.854E-12
      J=DCMPLX(0.0,1.0)
      Read(9,*) A
      Read(9,*) B
      Read(9,'(2D10.6)') Er
      Read(9,'(2D10.6)') Ur
      Read(9,*) Cond
      Read(9,*) K1
      Read(9,*) DeltaB
```

```
      Read(9,'(I2)') M
      Read(9,*) theta
      Read(9,'(I1)') POL
c  POL = 1 implies TM polarization
c  POL = 0 implies TE polarization
      theta=theta*PI/180.0
      Index=CDsqrt(Er*Ur+J*Ur*Cond/(K1*Eo*c))
      K2=K1*Index
      K2A=K2*A
      N=int(SQRT(Dreal(K2A)**2.+DIMAG(K2A)**2.)+20.)
      Call JNZ(K2A,JNK2A,J0K2A,N)
      Call YNZ(K2A,JNK2A,J0K2A,YNK2A,Y0K2A,N)
      Pr=Ur
      IF(POL.eq.0) Pr=Er
c
c main loop
c
      do 100 L=1,M
      K2B=K2*B
      K1B=K1*B
      B=B+DeltaB
      N=int(SQRT(Dreal(K2B)**2.+DIMAG(K2B)**2.))+20.
c
c  fill arrays with bessel functions
c
      Call JNX(K1B,JN,J0,N)
      Call JNZ(K2B,JNK2B,J0K2B,N)
      Call YNX(K1B,JN,J0,YNK1B,Y0K1B,N)
      Call YNZ(K2B,JNK2B,J0K2B,YNK2B,Y0K2B,N)
      If(POL.eq.1) THEN
        DN(1)=-YNK2B(1)*J0K2A+JNK2B(1)*Y0K2A
        DN(2)=Y0K2B*J0K2A-J0K2B*Y0K2A
      ELSE
        DN(1)=YNK2B(1)*JNK2A(1)-JNK2B(1)*YNK2A(1)
        DN(2)=-Y0K2B*JNK2A(1)+J0K2B*YNK2A(1)
      ENDIF
      ANN=Pr*JN(1)*DN(2)+J0*Index*DN(1)
      ANND=ANN+J*(Pr*DN(2)*YNK1B(1)+INDEX*DN(1)*Y0K1B)
      CDSUM=J*ANN/ANND*(-Y0K1B*JN(1)+J0*YNK1B(1))
      do 40 I=1,N-2
        X=DFLOAT(I)
        JNPM=X/K1B*JN(I)-JN(I+1)
        YNPK1B=X/K1B*YNK1B(I)-YNK1B(I+1)
        YNPK2B=X/K2B*YNK2B(I)-YNK2B(I+1)
        JNPK2B=X/K2B*JNK2B(I)-JNK2B(I+1)
        IF(POL.EQ.1) THEN
          DN(1)=YNPK2B*JNK2A(I)-JNPK2B*YNK2A(I)
          DN(2)=YNK2B(I)*JNK2A(I)-JNK2B(I)*YNK2A(I)
        ELSE
          YNPK2A=X/K2A*YNK2A(I)-YNK2A(I+1)
```

```
            JNPK2A=X/K2A*JNK2A(I)-JNK2A(I+1)
            DN(1)=YNPK2B*JNPK2A-JNPK2B*YNPK2A
            DN(2)=YNK2B(I)*JNPK2A-JNK2B(I)*YNPK2A
          ENDIF
        ANN=Index*JN(I)*DN(1)-Pr*JNPM*DN(2)
        ANND=ANN+J*(Index*YNK1B(I)*DN(1)-Pr*YNPK1B*DN(2))
        AN=J*ANN/ANND*(YNK1B(I)*JNPM-JN(I)*YNPK1B)
        CDSUM=CDSUM+2.0*AN*dcos(X*theta)
        IF(1.0E05*CDABS(AN).LT.CDABS(CDSUM))  goto 41
40      continue
41
Sigma=PI*K1B**2.0/2.0*(real(CDSUM)**2.0+IMAG(CDSUM)**2.0)
        write(8,*) K1B,Sigma
100     continue
        stop
        end
```

The next program is the OSRC approximation for the RCS of a dielectric coated cylinder using the first method described in Chapter 3.

```
c234567890
      Program OSRCV3
      Complex*16 JNK2B(101),J0K2B,JNK2A(101),J0K2A,ANN
      Complex*16 YNK2B(101),Y0K2B,YNK2A(101),Y0K2A,AN
      Complex*16 JNPK2B,YNPK2B,JNPK2A,YNPK2A,Index,K2,ANND
      Complex*16 K2A,K2B,CDSUM,J,DN(3),K1B1,DN30,Er,Ur,Pr
      Double Precision PI,J0,X,theta,JNC(101),J0C
      Double Precision JNPM,JN(101),YNK1B(101),Y0K1B,K1B
      Double Precision Cond,K1,A,B,Eo,c,DeltaB,YOFX
      Integer N,L,M,POL
      open(8,file='outv3.prn')
      open(9,file='inv2.dat')
c
c  Initialize constants
c
      PI=3.14159265
      c=3.0E+08
      Eo=8.854E-12
      J=DCMPLX(0.0,1.0)
      Read(9,*) A
      Read(9,*) B
      Read(9,'(2D10.6)') Er
      Read(9,'(2D10.6)') Ur
      Read(9,*) Cond
      Read(9,*) K1
```

```
      Read(9,*) DeltaB
      Read(9,'(I2)') M
      Read(9,*) theta
      Read(9,'(I1)') POL
c  POL = 1 implies TM polarization
c  POL = 0 implies TE polarization
      theta=theta*PI/180.0
      Index=CDsqrt(Er*Ur+J*Ur*Cond/(K1*Eo*c))
      K2=K1*Index
      K2A=K2*A
      N=int(SQRT(real(K2A)**2.+IMAG(K2A)**2.))+10.
      Call JNZ(K2A,JNK2A,J0K2A,N)
      Call YNZ(K2A,JNK2A,J0K2A,YNK2A,Y0K2A,N)
      Pr=Ur
      IF(POL.EQ.0) Pr=Er
c
c main loop
c
      do 100 L=1,M
      K2B=K2*B
      K1B=K1*B
      B=B+DeltaB
      K1B1=1.0-J*K1B
      N=int(SQRT(real(K2B)**2.+IMAG(K2B)**2.))+20.
c
c  fill arrays with bessel functions
c
      Call JNX(K1B,JN,J0,N)
      Call JNZ(K2B,JNK2B,J0K2B,N)
      Call YNX(K1B,JN,J0,YNK1B,Y0K1B,N)
      Call YNZ(K2B,JNK2B,J0K2B,YNK2B,Y0K2B,N)
      IF (POL.EQ.1) THEN
        DN(1)=-YNK2B(1)*J0K2A+JNK2B(1)*Y0K2A
        DN(2)=Y0K2B*J0K2A-J0K2B*Y0K2A
      ELSE
        DN(1)=YNK2B(1)*JNK2A(1)-JNK2B(1)*YNK2A(1)
        DN(2)=-Y0K2B*JNK2A(1)+J0K2B*YNK2A(1)
      ENDIF
      DN30=J-1.0/(2.0*K1B)+1.0/(8.0*K1B*K1B1)
      ANN=(-JN(1)-DN30*J0)**2.*DN(2)
      ANND=INDEX*DN(1)-Pr*DN(2)*DN30
      CDSUM=ANN/ANND
      do 40 I=1,N-2
        X=Dfloat(I)
        JNPM=X/K1B*JN(I)-JN(I+1)
        YNPK2B=X/K2B*YNK2B(I)-YNK2B(I+1)
        JNPK2B=X/K2B*JNK2B(I)-JNK2B(I+1)
        IF(POL.EQ.1) THEN
          DN(1)=YNPK2B*JNK2A(I)-JNPK2B*YNK2A(I)
          DN(2)=YNK2B(I)*JNK2A(I)-JNK2B(I)*YNK2A(I)
```

```
          ELSE
            YNPK2A=X/K2A*YNK2A(I)-YNK2A(I+1)
            JNPK2A=X/K2A*JNK2A(I)-JNK2A(I+1)
            DN(1)=YNPK2B*JNPK2A-JNPK2B*YNPK2A
            DN(2)=YNK2B(I)*JNPK2A-JNK2B(I)*YNPK2A
          ENDIF
          DN(3)=DN30-(X**2.0)/(2.0*K1B*K1B1)
          ANN=(JNPM-DN(3)*JN(I))**2.*DN(2)
          ANND=INDEX*DN(1)-Pr*DN(2)*DN(3)
          AN=ANN/ANND
          CDSUM=CDSUM+2.0*AN*Dcos(X*theta)
          IF(1.0E05*CABS(AN).LT.CABS(CDSUM))  goto 41
40      continue
41      X=2.0*dsin(theta/2.0)*K1B
        M=INT(X)+3.
        Call JNX(X,JNC,J0C,M)

CDSUM=Pr*CDSUM+(DN30-K1B/(4.0*K1B1))*J0C+(1.0+1/(2.0*K1B1))
     x*sin(theta/2.)*JNC(1)+K1B/(4.0*K1B1)*cos(theta)*JNC(2)

Sigma=PI*K1B**2.0/2.0*(Dreal(CDSUM)**2.0+DIMAG(CDSUM)**2.0)
        write(8,*) K1B,Sigma
100     continue
        stop
        end
```

The next program is the OSRC approximation for the RCS of a dielectric coated cylinder using the second method described in Chapter 3.

```
c234567890
        Program OSRCV5
        Complex*16 JNK2B(101),J0K2B,JNK2A(101),J0K2A,AN
        Complex*16 YNK2B(101),Y0K2B,YNK2A(101),Y0K2A,ANND
        Complex*16 JNPK2B,YNPK2B,JNPK2A,YNPK2A,Index,K2
        Complex*16 K2A,K2B,CDSUM,J,DN(3),K1B1,Er,Ur,Pr
        Complex*16 ANN,DN30
        Double Precision PI,J0,X,theta
        Double Precision JNPM,JN(101),YNK1B(101),Y0K1B,K1B
        Double Precision Cond,K1,A,B,Eo,c,DeltaB
        Integer N,L,M,POL
        open(8,file='outv5.prn')
        open(9,file='inv2.dat')
c
```

```
c  Initialize constants
c
      PI=3.14159265
      c=3.0E+08
      Eo=8.854E-12
      J=DCMPLX(0.0,1.0)
      Read(9,*) A
      Read(9,*) B
      Read(9,'(2D10.6)') Er
      Read(9,'(2D10.6)') Ur
      Read(9,*) Cond
      Read(9,*) K1
      Read(9,*) DeltaB
      Read(9,'(I2)') M
      Read(9,*) theta
      Read(9,'(I1)') POL
c  POL = 1 implies TM polarization
c  POL = 0 implies TE polarization
      theta=theta*PI/180.0
      Index=CDsqrt(Er*Ur+J*Ur*Cond/(K1*Eo*c))
      K2=K1*Index
      K2A=K2*A
      N=int(SQRT(real(K2A)**2.+IMAG(K2A)**2.))+20.
      Call JNZ(K2A,JNK2A,J0K2A,N)
      Call YNZ(K2A,JNK2A,J0K2A,YNK2A,Y0K2A,N)
      Pr=Ur
      IF(POL.EQ.0) Pr=Er
c
c main loop
c
      do 100 L=1,M
      K2B=K2*B
      K1B=K1*B
      B=B+DeltaB
      K1B1=1.0-J*K1B
      N=int(SQRT(real(K2B)**2.+IMAG(K2B)**2.))+20.
c
c  fill arrays with bessel functions
c
      Call JNX(K1B,JN,J0,N)
      Call JNZ(K2B,JNK2B,J0K2B,N)
      Call YNX(K1B,JN,J0,YNK1B,Y0K1B,N)
      Call YNZ(K2B,JNK2B,J0K2B,YNK2B,Y0K2B,N)
      IF (POL.EQ.1) THEN
        DN(1)=-YNK2B(1)*J0K2A+JNK2B(1)*Y0K2A
        DN(2)=Y0K2B*J0K2A-J0K2B*Y0K2A
      ELSE
        DN(1)=YNK2B(1)*JNK2A(1)-JNK2B(1)*YNK2A(1)
        DN(2)=-Y0K2B*JNK2A(1)+J0K2B*YNK2A(1)
      ENDIF
```

```
      DN30=J-1.0/(2.0*K1B)+1.0/(8.0*K1B*K1B1)
      ANN=(-JN(1)-DN30*J0)*(INDEX*DN(1)*J0+Pr*DN(2)*JN(1))
      ANND=INDEX*DN(1)-Pr*DN(2)*DN30
      CDSUM=ANN/ANND
      do 40 I=1,N-2
        X=DFloat(I)
        JNPM=X/K1B*JN(I)-JN(I+1)
        YNPK2B=X/K2B*YNK2B(I)-YNK2B(I+1)
        JNPK2B=X/K2B*JNK2B(I)-JNK2B(I+1)
        IF(POL.EQ.1) THEN
          DN(1)=YNPK2B*JNK2A(I)-JNPK2B*YNK2A(I)
          DN(2)=YNK2B(I)*JNK2A(I)-JNK2B(I)*YNK2A(I)
        ELSE
          YNPK2A=X/K2A*YNK2A(I)-YNK2A(I+1)
          JNPK2A=X/K2A*JNK2A(I)-JNK2A(I+1)
          DN(1)=YNPK2B*JNPK2A-JNPK2B*YNPK2A
          DN(2)=YNK2B(I)*JNPK2A-JNK2B(I)*YNPK2A
        ENDIF
        DN(3)=DN30-(X**2.0)/(2.0*K1B*K1B1)

ANN=(JNPM-DN(3)*JN(I))*(INDEX*DN(1)*JN(I)-Pr*DN(2)*JNPM)
        ANND=INDEX*DN(1)-Pr*DN(2)*DN(3)
        AN=ANN/ANND
        CDSUM=CDSUM+2.0*AN*cos(X*theta)
        IF(1.0E05*CABS(AN).LT.CABS(CDSUM))  goto 41
40    continue
41    continue

Sigma=PI*K1B**2.0/2.0*(real(CDSUM)**2.0+IMAG(CDSUM)**2.0)
      write(8,*) K1B,Sigma
100   continue
      stop
      end
```

The next program was used to calculate the error terms and coefficients of Equation 3.53 and Figures 36 and 37.

```
c234567890
      Program ERROR
      Complex*16 JNK2B(101),J0K2B,JNK2A(101),J0K2A,BN(3),YFC
      Complex*16 YNK2B(101),Y0K2B,YNK2A(101),Y0K2A,XN
      Complex*16 JNPK2B,YNPK2B,JNPK2A,YNPK2A,Index,K2,ANND
      Complex*16 K2A,K2B,CDSUM,J,DN(3),K1B1,DN30,Er,Ur,Pr
      Complex*16 YN,YNN,YNND,AN,AN,ANN
      Double Precision PI,J0,X,theta,JNC(101),J0C,YOFX
      Double Precision JNPM,JN(101),YNK1B(101),Y0K1B,K1B
      Double Precision Cond,K1,A,B,Eo,c,DeltaB
```

```
      Integer N,L,M,POL
      open(8,file='outv3.prn')
      open(9,file='inv2.dat')
      open(10,file='EN.prn')
      open(11,file='ENYN.prn')
      open(12,file='ENXN.prn')
      open(14,file='AN.prn')
      open(15,file='XNYN.prn')
c
c  Initialize constants
c
      PI=3.14159265
      c=3.0E+08
      Eo=8.854E-12
      J=DCMPLX(0.0,1.0)
      Read(9,*) A
      Read(9,*) B
      Read(9,'(2D10.6)') Er
      Read(9,'(2D10.6)') Ur
      Read(9,*) Cond
      Read(9,*) K1
      Read(9,*) DeltaB
      Read(9,'(I2)') M
      Read(9,*) theta
      Read(9,'(I1)') POL
c  POL = 1 implies TM polarization
c  POL = 0 implies TE polarization
      theta=theta*PI/180.0
      Index=CDsqrt(Er*Ur+J*Ur*Cond/(K1*Eo*c))
      K2=K1*Index
      K2A=K2*A
      N=int(SQRT(Dreal(K2A)**2.+DIMAG(K2A)**2.)+20.)
      Call JNZ(K2A,JNK2A,J0K2A,N)
      Call YNZ(K2A,JNK2A,J0K2A,YNK2A,Y0K2A,N)
      Pr=Ur
      IF(POL.eq.0) Pr=Er
c
c main loop
c
      do 100 L=1,M
      K2B=K2*B
      K1B=K1*B
      K1B1=1.0-J*K1B
      B=B+DeltaB
      N=int(SQRT(Dreal(K2B)**2.+DIMAG(K2B)**2.))+20.
c
c  fill arrays with bessel functions
c
      Call JNX(K1B,JN,J0,N)
      Call JNZ(K2B,JNK2B,J0K2B,N)
```

```
Call YNX(K1B,JN,J0,YNK1B,Y0K1B,N)
Call YNZ(K2B,JNK2B,J0K2B,YNK2B,Y0K2B,N)
If(POL.eq.1) THEN
  DN(1)=-YNK2B(1)*J0K2A+JNK2B(1)*Y0K2A
  DN(2)=Y0K2B*J0K2A-J0K2B*Y0K2A
ELSE
  DN(1)=YNK2B(1)*JNK2A(1)-JNK2B(1)*YNK2A(1)
  DN(2)=-Y0K2B*JNK2A(1)+J0K2B*YNK2A(1)
ENDIF
DN30=J-1.0/(2.0*K1B)+1.0/(8.0*K1B*K1B1)
BN(1)=(-JN(1)-J*YNK1B(1))
BN(2)=BN(1)/(J0+J*Y0K1B)
BN(3)=BN(2)-DN30
Xn=(BN(3)*Pr*DN(2))/(INDEX*DN(1)-Pr*DN(2)*BN(2))
ANN=Pr*JN(1)*DN(2)+J0*Index*DN(1)
ANND=ANN+J*(Pr*DN(2)*YNK1B(1)+INDEX*DN(1)*Y0K1B)
CDSUM=J*ANN/ANND*(-Y0K1B*JN(1)+J0*YNK1B(1))
YNN=-ANN*BN(2)*JN(1)-Pr*DN(2)*CDSUM
YND=ANN*(J0+BN(2)*JN(1))
YN=YNN/YND
write(12,*) XN*BN(3)*CDSUM
write(10,*) BN(3)*CDSUM
write(11,*) YN*BN(3)*CDSUM
write(14,*) cdsum
write(15,*) XN*YN*CDSUM*BN(3)
do 40 I=1,N-2
  X=DFLOAT(I)
  JNPM=X/K1B*JN(I)-JN(I+1)
  YNPK1B=X/K1B*YNK1B(I)-YNK1B(I+1)
  YNPK2B=X/K2B*YNK2B(I)-YNK2B(I+1)
  JNPK2B=X/K2B*JNK2B(I)-JNK2B(I+1)
  IF(POL.EQ.1) THEN
    DN(1)=YNPK2B*JNK2A(I)-JNPK2B*YNK2A(I)
    DN(2)=YNK2B(I)*JNK2A(I)-JNK2B(I)*YNK2A(I)
  ELSE
    YNPK2A=X/K2A*YNK2A(I)-YNK2A(I+1)
    JNPK2A=X/K2A*JNK2A(I)-JNK2A(I+1)
    DN(1)=YNPK2B*JNPK2A-JNPK2B*YNPK2A
    DN(2)=YNK2B(I)*JNPK2A-JNK2B(I)*YNPK2A
  ENDIF
DN(3)=DN30-(X**2.0)/(2.0*K1B*K1B1)
BN(1)=(JNPM+J*YNPK1B)
BN(2)=BN(1)/(Jn(I)+J*YNK1B(I))
BN(3)=BN(2)-DN(3)
Xn=(BN(3)*Pr*DN(2))/(INDEX*DN(1)-Pr*DN(2)*BN(2))
ANN=Index*JN(I)*DN(1)-Pr*JNPM*DN(2)
ANND=ANN+J*(Index*YNK1B(I)*DN(1)-Pr*YNPK1B*DN(2))
AN=J*ANN/ANND*(YNK1B(I)*JNPM-JN(I)*YNPK1B)
YNN=-ANN*BN(2)*JN(1)-Pr*DN(2)*AN
YND=ANN*(JN(I)-BN(2)*JNPM)
```

```
      YN=YNN/YND
      write(12,*) XN*BN(3)*AN
      write(10,*) BN(3)*AN
      write(11,*) YN*BN(3)*AN
      write(14,*) AN
      write(15,*) XN*YN*AN*BN(3)
      CDSUM=CDSUM+2.0*AN*dcos(X*theta)
      IF(1.0E05*CDABS(AN).LT.CDABS(CDSUM))  goto 41
40    continue
41
Sigma=PI*K1B**2.0/2.0*(real(CDSUM)**2.0+IMAG(CDSUM)**2.0)
      write(8,*) K1B,Sigma
100   continue
      stop
      end
```

Bibliography

Abromowitz, Milton and Stegun, Irene A. Handbook of Mathematical Functions. Dover Publications Inc., New York. 1965.

Baker, William. Class Notes from MATH 5.12, Mathematical Methods of Scattering. School of Engineering, Air Force Institute of Technology (AU), Wright-Patterson AFB OH, January 1988.

Bowman, J.J. et al., Eds. Electromagnetic and Acoustic Scattering by Simple Shapes. Amsterdam: North-Holland Publishing Company. 1969.

Chang, Shu-Kong and Kenneth K. Mei. "Application of the Unimoment Method to Electromagnetic Scattering of Dielectric Cylinders," IEEE Transactions on Antennas and Propagation, 25: 35-42 (January 1976)

Colton, David and Kress, Rainer. Integral Equations Methods in Scattering Theory. Wiley and Sons, New York. 1983.

Gradshteyn, I. S. and Ryzhik, I. M. Table of Integrals, Series, and Products. Academic Press, New York. 1980.

Harrington Roger F. Time-Harmonic Electromagnetic Fields. McGraw Hill Book Co., New York. 1961.

------ High Loss Dielectrics Microwave Absorbers. Eccosorb Product Catalog, Emerson and Cummings, Canton MA. 1980.

James, Graeme L. Geometrical Theory of Diffraction for Electromagnetic Waves. Stevenage, England, Peter Peregrinus Ltd. 1976.

Jin, Jian-Ming and Valdis V. Liepa. "Application of Hybrid Finite Element Method to Electromagnetic Scattering from Coated Cylinders," IEEE Transactions on Antennas and Propagation, 36: 50-54 (January 1988)

Joseph, Lt John. Multiple Angles of Incidence Measurement Technique for the Permittivity and Permeability of Lossy Material at Millimeter Wavelengths. MS Thesis AFIT/GE/ENG/86D-58. School of Engineering, Air Force Institute of Technology (AU), Wright Patterson AFB OH, December 1986.

Jost Randy J. Class Notes from EENG 6.30, Applications of Electromagnetic Theory. School of Engineering, Air Force Institute of Technology (AU), Wright-Patterson AFB OH, January 1988.

Kelly, Louis G. Handbook of Numerical Methods and Applications. Addison-Wesley Co. Reading, MA. 1967.

Knott Eugene F. and others. Radar Cross Section. Artech House, Inc. Norwood MA. 1985.

Kriegsman, Gregory A. and Cathleen S. Morawetz. "Solving the Helmholtz Equation for Exterior Problems with Variable Index of Refraction : I," SIAM Journal for Scientific and Statistical Computation, 1: 371-385 (September 1980)

Kriegsman, Gregory A. et al. "A New Formulation of Electromagnetic Scattering Using an On-Surface Radiation Boundary Condition Approach," IEEE Transactions on Antennas and Propagation, 35: 153-161 (February 1987)

Leader Carl J. "Modern Methods of Scattering Predictions," Proceedings of SPIE - The International Society for Optical Engineering, Applications of Mathematics in Modern Optics, 358: 17-23 (August 1982)

Peters, Leon Jr. "End-Fire Echo Area of Long Thin Bodies," IRE Transactions on Antennas and Propagation, 1: 133-139 (January 1958)

Ruck G. T. et al. Radar Cross Section Handbook. Plenum Press, New York. 1970.

Tang, Charles C. H. "Backscattering from Dielectric-Coated Infinite Cylindrical Obstacles," Journal of Applied Physics, 28: 628-633 (May 1957)

Wang, Nan. "Electromagnetic Scattering from a Dielectric-Coated Circular Cylinder," IEEE Transactions on Antennas and Propagation, 33: 960-963 (September 1985)

Wu, Te-Hao and Leonard L.Tsai. "Scattering by Arbitrarily Cross-Sectioned Layered Dielectric Cylinders," IEEE Transactions on Antennas and Propagation, 25: 518-524 (July 1977)

VITA

Captain William Oetting was born on [redacted] He graduated from high school in [redacted] 1974. He enlisted in the Air Force in 1978 and was selected to attended the University of Washington, Seattle, Washington under the Airmans Education and Commissioning Program. He graduated Magna Cum Laude in December 1983 with a Bachelor of Science in Electrical Engineering and was commissioned in April 1984 after completing Officers Training School at Lackland AFB, Texas. Before entering the School of Engineering, Air force Institute of Technology, he worked for three years at the Air Force Wright Aeronautical Laboratories, Avionics Laboratory as a electronic warfare research engineer.

[redacted]

UNCLASSIFIED
SECURITY CLASSIFICATION OF THIS PAGE

REPORT DOCUMENTATION PAGE

Form Approved OMB No. 0704-0188

1a. REPORT SECURITY CLASSIFICATION: UNCLASSIFIED	1b. RESTRICTIVE MARKINGS
2a. SECURITY CLASSIFICATION AUTHORITY	3. DISTRIBUTION/AVAILABILITY OF REPORT: Approved for Public Release; Distribution Unlimited
2b. DECLASSIFICATION/DOWNGRADING SCHEDULE	
4. PERFORMING ORGANIZATION REPORT NUMBER(S): AFIT/MA/GE/88D-2	5. MONITORING ORGANIZATION REPORT NUMBER(S)
6a. NAME OF PERFORMING ORGANIZATION: School of Engineering; 6b. OFFICE SYMBOL (If applicable): AFIT/ENA	7a. NAME OF MONITORING ORGANIZATION
6c. ADDRESS (City, State, and ZIP Code): Air Force Institute of Technology, Wright-Patterson AFB, Ohio 45433	7b. ADDRESS (City, State, and ZIP Code)
8a. NAME OF FUNDING/SPONSORING ORGANIZATION: Air Force Wright Aeronautical Laboratories; 8b. OFFICE SYMBOL (If applicable): AFWAL/CDJ	9. PROCUREMENT INSTRUMENT IDENTIFICATION NUMBER
8c. ADDRESS (City, State, and ZIP Code): WPAFB, Ohio 45433	10. SOURCE OF FUNDING NUMBERS: PROGRAM ELEMENT NO. / PROJECT NO. / TASK NO. / WORK UNIT ACCESSION NO.

11. TITLE (Include Security Classification)
The Radar Cross Section of a Two Dimensional Dielectric Coated Cylinder Using On-Surface Radiation Conditions UNCLASSIFIED

12. PERSONAL AUTHOR(S)
William D. Oetting, Capt. USAF

13a. TYPE OF REPORT	13b. TIME COVERED	14. DATE OF REPORT (Year, Month, Day)	15. PAGE COUNT
MS Thesis	FROM _____ TO _____	1988 December	115

16. SUPPLEMENTARY NOTATION

17. COSATI CODES			18. SUBJECT TERMS (Continue on reverse if necessary and identify by block number)
FIELD	GROUP	SUB-GROUP	
12	02		Radar Cross Sections, Electromagnetic Scattering, Electromagnetic Theory, Scattering Cross Sections
17	09		

19. ABSTRACT (Continue on reverse if necessary and identify by block number)

Thesis Chairman: William Baker, Lt Col, USAF
Assistant Professor of Applied Mathematics

Abstract:
The RCS of a dielectric coated circular cylinder was found using an On-Surface Radiation Condition (OSRC) and compared to a eigenfunction solution. The OSRC approximation was found to agree with the eigenfunction solution whenever the higher order modes of the field in the dielectric layer were insignificant. An electrically thin layer or a resonable amount of loss in the dielectric material would produce an accurate OSRC approximation for resonant size scatterers. Specific results indicated that the magnitude of the imaginary part of the relative permittivity should be greater than 1.0 for an accurate approximation.

20. DISTRIBUTION/AVAILABILITY OF ABSTRACT	21. ABSTRACT SECURITY CLASSIFICATION
☐ UNCLASSIFIED/UNLIMITED ☒ SAME AS RPT. ☐ DTIC USERS	UNCLASSIFIED
22a. NAME OF RESPONSIBLE INDIVIDUAL: Lt Col William Baker	22b. TELEPHONE (Include Area Code): 513-255-4185 / 22c. OFFICE SYMBOL: AFIT/MA

DD Form 1473, JUN 86 *Previous editions are obsolete.*

SECURITY CLASSIFICATION OF THIS PAGE
UNCLASSIFIED